Tampere University

Humayra Anjumee Jeba

DISTINGUISHING MICROMOBILITY AND BLOCKAGE IN 6G SUB-THZ SYSTEMS

A machine learning approach

Faculty of Information Technology and Communication Sciences (ITC)
Master's thesis
August 2025

Abstract

Humayra Anjumee Jeba: Distinguishing Micromobility and Blockage in 6G Sub-THz Systems: A machine learning approach
Master's Thesis
Tampere University
Master's Degree Programme in Communication Systems and Networks
August 2025

As wireless communication expands, 6G is expected to restructure connectivity by enabling ultra-reliable, high-speed links across sub-terahertz(sub-THz) frequencies. These systems will play an important role in supporting advanced applications like holographic communication, extended reality and automation. However, connectivity in 6G networks is highly sensitive to physical impairments such as human body blockage and device micromobility. These two phenomena trigger different recovery procedures, making it essential to distinguish between them rapidly and accurately to maintain proper service and optimize resource allocation. In this thesis, we developed a machine-learning based statistical interference framework to proactively differentiate between blockage and micromobility events using measurements collected at 156 GHz. Our methodology included generating synthetic signal traces, training multiple classifier models, autoencoder and comparing their performance using standard evolution metrics. The result shows that ensemble models, particularly Random Forest which achieve up to 95% classification accuracy, outperforming more complex approaches in both accuracy and reliability. From here it confirms that lightweight models can support real-time decision-making and enable strong, proactive connectivity management in future 6G deployments.

Keywords: 6G, mmWave, sub-terahertz, micromobility, blockage detection, machine learning models, random forest, autoencoder.

The total word count of this thesis is words.

The originality of this thesis has been checked using the Turnitin Originality Check service.

Use of Artificial Intelligence

I hereby declare that the following AI-based tools were used in the preparation of this thesis:

Applications and Versions:

- ChatGPT (GPT-4-turbo)
- Claude Sonnet (version 4.0)

Purpose of AI Usage: These revisions assist with grammatical correctness and formatting consistency. They also improve paragraph coherence and language fluency.

Chapters and Sections Where AI Was Used:

- Literature review in Chapter 1.
- Formatting assistance in LaTeX for Chapters 3 and 4.
- Refinement of the Performance Assessment section in Chapter 4.

Acknowledgement of Responsibility and Risks:

As the author of this thesis, I take full responsibility for all the work presented here. While I used AI tools to help with grammar, writing clarity, and formatting, I made all the important academic choices myself. This includes deciding which sources to use, how to conduct my research, how to analyze my findings, and what conclusions to draw. I understand that I am fully accountable for this work and any issues that might arise from using AI assistance.

Preface

Nearly two years ago, I arrived in Finland with a dream to open new academic avenues for myself. This journey provided me with opportunities to explore integrative topics and approach problems from a multidisciplinary perspective, inevitably leading me to research experiences in computer networks. Tampere University delivered on its promise of comprehensive and forward-thinking education, providing the intellectual foundation that shaped this work.

I will be forever grateful to Dr. Dimitri Moltchanov, whose constant support and guidance were pivotal to my tremendous growth throughout this research journey. His constant encouragement provided me with the solid mindset necessary to overcome the challenging transition from job searching to establishing myself in the research field. I cannot thank Anna Gaidamaka enough for her immense support during this thesis work. From her, I learned the invaluable skill of managing multiple responsibilities while maintaining composure. She helped me synchronize all aspects of my research and academic life.

Finally, I am deeply thankful to my parents and my three cherished sisters for their unwavering support throughout this transformative period. They have been my source of strength and inspiration. It is to them that I dedicate this thesis.

Tampere University
Humayra Anjumee Jeba
Master's Degree Programme in Communication Systems and Networks
August 2025

Conflict of Interest Statement

The author declares that there are no conflicts of interest regarding the publication of this thesis. The research was conducted in the absence of any commercial or financial relationships that could be construed as a potential conflict of interest.

Author Contributions

This thesis represents the original work of Humayra Anjumee Jeba. The research design, methodology, data collection, analysis, and interpretation were conducted independently by the author under the supervision of Dr. Dimitri Moltchanov and with guidance from Anna Gaidamaka. All written content, including literature review, theoretical framework, and conclusions, are the original contributions of the author.

Ethics Statement

This research was conducted in accordance with the ethical standards and guidelines established by Tampere University. The study did not involve human subjects, animal testing, or sensitive data that would require specific ethical approval. All research methodologies employed were in compliance with international standards for academic research integrity and responsible conduct of research.

Funding Statement

This thesis work was completed as part of the author's degree program at Tampere University. No external funding or grants were received specifically for this research project. The research was supported by the institutional resources and facilities provided by Tampere University.

Contents

List of Figures

List of Tables

List of Abbreviations

3GPP	3rd Generation Partnership Project
5G	Fifth-generation
AI	Artificial Intelligence
AR	Augmented Reality
AEs	Autoencoders
BS	Base Station
CA	Carrier Aggregation
CNNs	Convolutional Neural Networks
DC	Dual Connectivity
DNNs	Deep Neural Networks
DSS	Dynamic Spectrum Sharing
eMBB	Enhanced Mobile Broadband
FFT	Fast Fourier Transform
FR1	Frequency Range 1 (up to 6 GHz)
FR2	Frequency Range 2 (24.25–52.6 GHz)
Gbps	Gigabits per second
GHz	Gigahertz
HPBW	Half-Power Beamwidth
HAPS	High-Altitude Platform Stations
HSPA	High-Speed Packet Access
IoT	Internet of Things
ITU IMT-2020	International Telecommunication Union International Mobile Telecommunications-2020
LSTM	Long Short-Term Memory
LoS	Line-of-Sight
LTE	Long Term Evolution
MAE	Mean Absolute Error
MCS	Modulation and Coding Scheme
Mbps	Megabits per second
MIMO	Multiple-Input Multiple-Output
ML	Machine Learning
MR-MC	Multi-Radio Multi-Connectivity
MSE	Mean Squared Error
mMTC	Massive Machine-Type Communication
NR	New Radio
NSA	Non-Stand-Alone
NTNs	Non-Terrestrial Networks

OFDM	Orthogonal Frequency-Division Multiplexing
QoS	Quality of Service
RE	Reconstruction Error
ReLU	Rectified Linear Unit
RNNs	Recurrent Neural Networks
Rx	Receiver
SRP	Signal Reception Probability
STD	Standard Deviation
sub-6 GHz	Frequencies below 6 Gigahertz
sub-THz	Sub-Terahertz
tanh	Hyperbolic Tangent Function
THz	Terahertz
Tx	Transmitter
UE	User Equipment
URLLC	Ultra-Reliable Low Latency Communication
VR	Virtual Reality
XGBoost	Extreme Gradient Boosting
XR	Extended Reality (AR/VR)

1 Introduction

Emerging wireless communication systems like 5G (30-70 GHz) and upcoming 6G (100-300 GHz) offer incredibly fast data speeds, but face significant challenges when users interact with their devices. However, these high-frequency signals are highly susceptible to challenges caused by user-induced factors. Our research focuses on two critical user-related problems that particularly affect these networks: human body blockage (when a person physically blocks the signal path) and micromobility (small movements of a handheld device). Both issues can dramatically impact connection quality or even cause complete signal loss, but they differ fundamentally in their characteristics and required solutions. Blockage, such as a user's hand or body temporarily obstructing the signal path, typically requires switching to a new base station to restore connectivity. In contrast, micromobility situations can usually be addressed through beam management techniques, such as rapid adjustment of beam direction or implementing more sophisticated beam tracking algorithms. The distinction is crucial because applying the wrong solution wastes valuable network resources and extends service disruption time, negatively affecting user experience. Mistaking one problem for the other leads to inefficient solutions or extended connection losses.

Given the ultra-fast rate of these networks, the system must identify and respond to these disruptions almost instantaneously. This approach enables preventive measures rather than reactive responses, significantly improving connection reliability and user satisfaction. To achieve this classification capability, we evaluated various machine learning approaches, testing their ability to distinguish between micromobility scenarios and blockage events based on signal characteristics. The research revealed that ensemble learning methods, particularly Random Forest algorithms, deliver superior performance in this application. These methods combine multiple decision trees to produce more accurate and robust predictions than single-algorithm approaches.

Our approach leverages measured Signal Reception Probability (SRP) traces at 156 GHz, collected separately for each impairment type, and synthesizes a combined time-series dataset containing both phenomena. The research on wireless communication blocking has had minimal attention in the THz range during recent years. The current procedures split detection techniques into online procedures and offline procedures. Complete statistical data enables offline detection techniques to produce accurate results for identifying blockage characteristics from rise time through fall time and duration. These methods cannot be used effectively for real-time operations because they provide detailed precision.

The purpose of online blockage detection is to instantly locate blockages, so adaptive MCS mechanisms use fast modifications to reduce signal degradation. Real-time data used by online approaches remains limited, which produces two detection problems: decreased precision together with increased delay time. Multiple researchers have demonstrated different machine learning techniques used for blockage identification processes. Deep Neural Networks (DNNs) with ReLU activation functions serve to identify blockages at three carrier frequencies that range from 30 to 48 GHz and end at 60 GHz. The research demonstrates an outstanding blockage detection accuracy between 0.9 and 0.98 based on the combination of network design and training information. Incorporation of LSTM neural networks in certain methods leads to dynamic parameter adjustments through historical blockage data for a detection accuracy improvement of up to 0.97. More powerful neural network layers at sub-6 GHz channels lead to greater probability of detection according to recent studies.

Although progress has been made, researchers still lack sufficient investigations on THz band blockage detection. The practical implementation of THz band systems encounters difficulties due to the lack of critical performance evaluation methods for detection latency and false alarm rate. Blockage detection analysis today functions as a black-box system since ML techniques get directly applied without studying how they affect detection performance.

1.1 Evolution of Wireless Communication cellular Technologies

Wireless communication technology have advanced significantly over the past few generations, changing how people connect with one other and converse. The proliferation of mobile broadband reflects a societal shift towards constant connectivity, with HSPA and LTE technologies emerging as primary enablers of this ubiquitous access paradigm. LTE infrastructure significantly enhances the user experience, supporting high-demand applications such as immersive multimedia, mobile content creation, and real-time professional communication platforms. One of LTE's pivotal advancements lies in its capability to deliver downlink speeds exceeding 100 Mbps, thereby expanding both user bandwidth capacity and the operational scalability of network providers. While 3G represents the prevailing mobile communication standard, 4G introduces a successor framework designed to elevate mobile data throughput and service convergence to next-generation benchmarks. For a system to meet true 4G criteria, it must achieve data transfer rates of 100 Mbps in mobile conditions and scale up to 1 Gbps in fixed scenarios, thus setting a new threshold for high-speed wireless communication. Unlike its predecessor, which employs a hy-

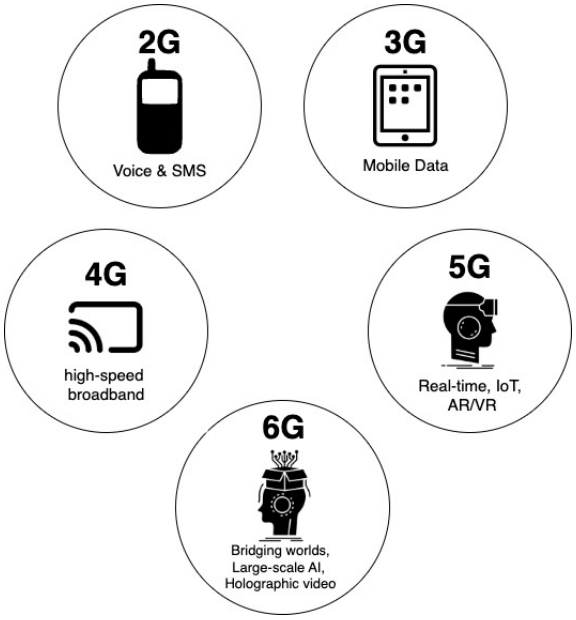

Figure 1.1 *Timeline of Wireless Communication Technologies*

brid of circuit- and packet-switching, 4G networks adopt a purely packet-switched architecture, optimizing bandwidth utilization and latency-sensitive service delivery. 4G technology represents a transformative leap in wireless communication, facilitating a seamless shift toward an all-encompassing wireless ecosystem with implications across both personal and professional spheres. [2] Fifth-generation (5G) mobile communication technology has introduced a fundamental shift in networking foundations, especially because of the noteworthy influence it has on IoT.

5G networks contrast with prior generations because they were purposely built to maintain connectivity for a tremendous number of devices, all while guaranteeing the high reliability and low latency inherent in such applications. Such a jump in network capability is required to foster a new wave of intelligent services spanning smart cities, autonomous vehicles, precision healthcare, and digital industry. [3] [4] At the foundation of 5G's framework are significant innovations, including massive machine-type connectivity, continual spectrum adjustment, and state-of-the-art MIMO antenna systems. These improvements, working together, result in exceptional flexibility and robustness within the network structure. Enabling adaptive, scalable, and energy-efficient operation, the network concept includes decoupled control and user interfaces, refined resource handling, and a sound architecture for small cell integration and inter-cell collaboration. [3]

Moreover, 5G integration with IoT platforms provides enhanced connectivity, reduced latency, and increased device density support compared to previous generation networks. It facilitates real-time data transfer, supports the proliferation of smart sensors and wearables, and addresses the massive data throughput demands

inherent in modern digital ecosystems. The convergence of these technologies is driving fundamental changes in connectivity models, thereby fostering innovation in sectors like healthcare, urban infrastructure, and advanced manufacturing. As the deployment of 5G progresses globally, it is expected to not only resolve limitations such as latency and bandwidth congestion seen in previous generations but also to set the foundation for future digital economies by underpinning emerging technologies like augmented and virtual reality, edge computing, and distributed AI applications. [4]

1.2 Fundamentals of 5G Technology

The upgrade from 4G LTE to 5G New Radio (NR) is distinguished by numerous architectural and performance capability shifts. The major change in this regard is the transition to directional wireless transmission at millimeter wave (mmWave) frequencies. Unlike its counterpart LTE, which is confined within the range of microwave spectrum, 5G NR extends to two frequency ranges – FR1 (up to 6 GHz) and FR2 (above 24.25 GHz up to 52.6 GHz) – the later being used for high-capacity data transmission at speeds of multiple gigabits per second. [5] Finding solutions to these issues, the 3rd Generation Partnership Project (3GPP) introduced the NR technology with massive MIMO, beamforming, a highly flexible frame structure, etc. These increments accommodate multitude deployment scenarios and are optimized for the ultra-low latency communication, for sub-1 ms round-trip times at the air interface, an improvement unrealizable in LTE [6]. 5G NR standardization began with Release 15, finalized in 2018, which initially enabled mmWave operation in non-stand-alone (NSA) mode. Release 16, completed in 2020, introduced key improvements including better MIMO and beamforming techniques, dynamic spectrum sharing (DSS), dual connectivity (DC), carrier aggregation (CA), and improved energy efficiency for user devices [7]. The significance of these developments was underscored when both Release 15 and 16 were officially recognized as part of the ITU IMT-2020 5G standard in July 2020 [8].

Furthermore, Release 17 broadens 5G NR's scope across three use-case families: enhanced mobile broadband (eMBB), ultra-reliable low latency communication (URLLC), and massive machine-type communications (mMTC). It introduces support for additional spectrum, access to the 60 GHz unlicensed band, new OFDM numerologies, channel access mechanisms, and functionalities tailored to XR (AR/VR) applications. It also supports reduced-capability user equipment to enhance mMTC deployment. NR also differs markedly from LTE in terms of resource management. It employs scalable numerologies for flexible time-frequency allocation, and it brings significant advancements in initial access, synchronization, channel coding, and modulation strategies [9]. As 3GPP prepares Release 18 and future iterations,

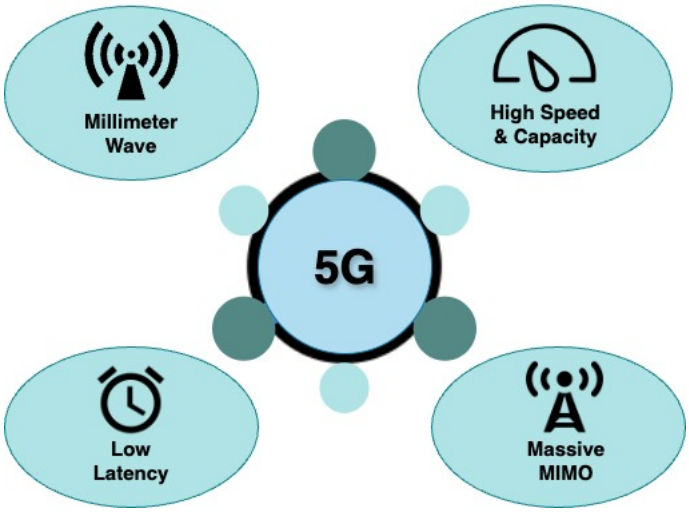

Figure 1.2 *5G value added specific features.*

additional research is addressing challenges such as beam management, network energy efficiency, seamless mobility, and operation above 52.6 GHz. Notably, future NR enhancements will also extend into non-terrestrial networks (NTNs), improved sidelink communication, power-saving features, and support for advanced broadcast and multicast services [10]. Thus, while LTE laid the groundwork for mobile broadband, 5G NR redefines the wireless paradigm, offering a flexible, scalable, and ultra-efficient platform capable of supporting the next generation of intelligent and immersive digital services. Integration of mmWave communication in next-generation 5G mobile networks has attracted a lot of attention from the industry and academia. At the center of this evolution, there is multi-connectivity, which is expected to play a vital part in boosting session continuity when the network is dynamic. As the community is actively determining the fundamental aspects of mmWave cellular systems and unraveling the mysteries of mmWave propagation attributes, there is critical need for evaluation methodologies that can evaluate session-level dynamics in real life deployments.

To address this demand, [11] proposed an integrated evaluation framework that assesses performance from both user and network perspectives. Such methodology is specifically optimized for mmWave situations in real urban conditions and adopts the crucial components, including: the structural conditions of mmWave channels, the time-varying blockage of LoS routes by human motion, and the cross-cell allocation of resources in the context of mmWave bands. A case study was conducted on a real scenario Manhattan grid at 28 GHz where the analysis of viable multi-connectivity mechanisms could be carried out at the depth [11]. Directional beamforming is a fundamental enabler for mmWave systems, integrated to counteract the inherently high path loss observed at these frequencies .The interference behavior and susceptibility to misaligned beams are drastically altered by the extremely directional

nature of mmWave beams, which resemble flashlights. [12] By concentrating energy in specific directions, beamforming significantly enhances signal strength and spatial selectivity [13]. However, this technique also necessitates specialized interference modeling approaches. In particular, [14] presents a robust and computationally efficient beamformer design using iterative fast Fourier transform (FFT) methods, while [15] introduces an interference cancellation-based hybrid precoding scheme that achieves performance close to optimal in mmWave MIMO systems.

Massive Multiple Input Multiple Output (MIMO) architectures further amplify the advantages of beamforming, offering the potential to deliver high data rates in dense mmWave deployments. Advanced modeling efforts, such as evaluate the spectral efficiency in two-tier heterogeneous network topologies, combining MIMO-equipped macro base stations with small cell overlays. Moreover, energy and spectral efficiency trade-offs in multi-cell, multi-user beamforming designs. Despite these advances, mmWave systems face critical challenges related to line-of-sight (LoS) signal integrity, particularly in urban environments. Recognizing human blockage as a significant propagation impediment, 3GPP incorporated relevant models in Technical Report 38.901 of Release 14 [16]. Real-world obstacles, including mobile entities like pedestrians and vehicles, can introduce abrupt signal attenuation of up to 30–40 dB. These blockages not only degrade performance but also add stochastic variability to the channel due to their mobility and random physical dimensions. Notably, 3GPP has emphasized the need for both spatial and temporal consistency in channel modeling, given that propagation conditions can change rapidly and unpredictably with each simulation instance [13].

1.3 Towards 6G: Vision and Technical Landscape

The performance of 5G wireless communication systems has been greatly improved due to the application of high-frequency technologies, i.e., millimeter-wave (mm-wave) communications. Due to the conflict between the fast growing demand for high data rate services and the limited spectrum resources, 5G may soon face its performance bottleneck. As a result, THz communications are being evaluated as one of the essential technologies for 6G systems [17].The mmWave spectrum, typically ranging from 30 to 70 GHz, has been a focal point in the evolution of wireless communications due to its vast available bandwidth and potential to deliver multi-gigabit data rates. One of the most significant impediments to mmWave deployment is its high sensitivity to blockage. Electromagnetic waves at these frequencies have a limited ability to diffract around obstacles, especially those larger than their wavelength. As a result, common elements in urban and indoor environments such as walls, furniture, and even human bodies can severely degrade signal strength. For

instance, blockage by a human alone can reduce the link budget by 20–30 dB. Additionally, mmWave suffers from higher free-space propagation losses compared to sub-6 GHz frequencies. Specifically, at 60 GHz, the propagation loss is approximately 28 dB greater than at 2.4 GHz due to the wavelength differential [18].

Micro-mobility, or the small-scale movement of users or devices within a service area, presents another significant difficulty. In order to overcome propagation losses, mmWave communication mostly depends on directional, narrow beams for both transmission and receiving. Beam training methods, which are sensitive to fast movement and time-consuming, are required to properly align these beams. Performance degradation or frequent disconnections can result from misalignment caused by even small user movement. In locations with high population density, where users and impediments are constantly moving, this issue is exacerbated. In order to maintain consistent coverage, mmWave communication requires a dense deployment of base stations (BSs) due to the high attenuation and poor diffraction qualities. However, this technique is not commercially feasible due to the expense and logistical difficulty of establishing fiber-based backhaul for every BS. There have been proposals for wireless backhaul solutions in mmWave frequencies such as 60 GHz and E-band (71–76 and 81–86 GHz), however their effectiveness is limited by the same propagation problems. In order to maintain consistent coverage, mmWave communication requires a dense deployment of base stations (BSs) due to the high attenuation and poor diffraction qualities. However, this technique is not commercially feasible due to the expense and logistical difficulty of establishing fiber-based backhaul for every BS. There have been proposals for wireless backhaul solutions in mmWave frequencies such as 60 GHz and E-band (71–76 and 81–86 GHz), however their effectiveness is limited by the same propagation problems [19].

The limited practical deployment of mmWave in 5G networks can be explained by the fact that these basic obstacles have not been addressed. The issue gets even more dire as we look to 6G. Even higher frequencies, such the THz band, which bears all of mmWave's drawbacks but to a greater extent, are planned for inclusion in emerging 6G systems. In THz systems, blockage leads to even greater attenuation, and because micro-mobility necessitates very narrow beam widths, beam miss alignments occur more frequently. Therefore, instead of being fixed, these problems get worse in 6G, necessitating a paradigm change in session continuity and radio access technology [20]. 6G networks are expected to achieve superior performance compared to 5G through the integration of advanced technologies, optimized system architectures, and AI-enhanced network management algorithms. With the use of terahertz and optical communication technologies, 6G will further improve high-frequency operation, which 5G has already pushed through mmWave bands. It is anticipated that 6G networks would shift from conventional cell-based designs

towards cell-less architectures that integrate numerous access and backhaul technologies in order to accommodate the variety of future applications and provide seamless 3D coverage. Additionally, intelligence will be embedded more deeply into the network, shifting from centralized cloud processing to distributed learning at the edge, enabling real-time predictions and autonomous adaptation. Unlike 5G, which balances performance trade-offs across applications, 6G aims to simultaneously meet ultra-high reliability, extreme capacity, energy efficiency, and low-latency demands in a unified and holistic manner tailored for the complex socioeconomic and technological landscape of the 2030s [21].

1.4 Literature Review

1.4.1 Micromobility Impairments

The evolution of wireless connectivity in 6G systems aims to achieve extreme capacity with peak data rates up to 1 Tbps and support broadband connectivity at high speeds [22]. MmWave communications in 5G systems face challenges due to frequent link blockages, leading to session drops. To improve session continuity, researchers have proposed bandwidth reservation and multi-connectivity techniques. Bandwidth reservation allocates a small portion of resources for ongoing sessions, significantly enhancing their continuity [23]. Key enablers include ultra-massive MIMO, intelligent reflecting surfaces, and integrated space and terrestrial networks. Multi-radio multi-connectivity (MR-MC) is proposed to enhance reliability and low latency in Sub-THz bands by allowing users to connect to different bands simultaneously [24]. 6G will also focus on massive machine-type communication (mMTC) and ultra-reliable low-latency communications (URLLC), with an emphasis on closed-loop massive connectivity and diverse safety-critical control applications [25]. To achieve these goals, 6G systems will utilize a wide spectrum range, from sub-6 GHz to (sub-)Terahertz and visible light communications, along with advanced coding, modulation, and waveforms to improve latency, reliability, and complexity [22].

In the context of Terahertz (THz) cellular systems, user micromobility represents a critical challenge distinct from static blockage, primarily due to the highly directional nature of THz communication. Micromobility specifically refers to the occasional rotations and small displacements of user equipment (UE) while held by a user. Unlike static blockages, which are fixed physical obstructions, micromobility is a dynamic phenomenon inherent to human-device interaction. This small-scale, continuous movement is particularly problematic for THz systems utilizing large antenna arrays, as it leads to beam misalignment and subsequent signal degradation. The performance impact of micromobility is often assessed by the ”time to the outage,” highlighting how these dynamic user movements directly contribute to

service interruptions [26].

3GPP has pointed out this challenge as its latest solution is multi-connectivity. Because of this, a user equipment (UE) is able to work through a blocked NR base station (BS) by connecting to one of the nearby alternate NR base stations [27]. In the systems being developed for New Radio (NR), when crowds move and block mmWave pathways, it is necessary to use smart ways to maintain session continuity. Guards are allocated at the NR base stations only for approved sessions, and this is done to help improve user experience by keeping the chances of newly initiated and ongoing sessions being rejected balanced [28]. Attention toward broadband high-altitude platform stations (HAPS) from 6G researchers comes from their ability to provide better LoS qualities and be effective at higher frequency bands like mmWave. To make mmWave base stations work with MIMO beamforming, the communication paths must be kept in a spatial line-of-site relationship. So, being able to control both the transmitters and receivers efficiently is essential.The use of beamforming is common in mmWave bands as it helps improve the effectiveness of mmWave radio networks. By using these methods, you can direct the signal's energy to a specific location [29].

1.4.2 Blockage Impairments

blockage, particularly from human bodies, is a critical factor limiting performance in mmWave/sub-THz systems, necessitating dynamic, time-dependent modeling approaches that account for both macro- and micro-mobility, as well as realistic antenna patterns and propagation effects [30] . One of the main problems that lower mmWave system performance is when there is blockage in the human body. Research evidence indicates that barriers can cause intermittent access to the wireless network as the obstacles in the environment move and interfere with the signal. Mobility among people in cities causes this change from blocked LoS to open LoS and back. The deployment of mmWave technology in 5G and beyond cellular networks has introduced significant challenges related to signal blockage [31]. Many realize that since mmWave waves are very small, they follow a different pattern of propagation from today's wireless bands. For instance, mmWave signals are affected by more pathloss, atmosphere attenuation, and diffraction than microwave systems are [32]. System developers face big challenges because they must make sure 5G NR systems offer solid and reliable connectivity. Many kinds of mobile objects, for instance cars and people, in the channel blocking the isolated channels can cause the signal to degrade or even to lead to an imbalance in ongoing sessions.

One of the main obstacles preventing mm Wave communications from offering ultra-high data rates and ultra-low latency networks is human blockage, which significantly lowers the quality-of-service (QoS) that users experience [33]. Both mmWave

and THz access systems are subject to the same type of impairments extremely large free-space propagation losses and blockage phenomenon. The principle difference is the magnitude of this effect with blockage causing much higher attenuation in THz band [34]. Conventionally, the performance of 5G/6G mmWave/sub-THz systems has been evaluated using static user location distributions, assuming continuous beam alignment through tracking procedures. [30]

1.5 Research Motivation & Questions

Based on the discussion about the challenges faced by high-frequency wireless systems, it is evident that detecting human body blockage is an important problem not only for 5G but for 6G as well. The transition to higher frequency bands like mmWave and sub-THz, while offering significant advantages in terms of bandwidth and data rates, introduces new complexities in signal propagation. Differenciating accurately between various forms of obstructions is especially important in situations where user equipment (UE) is being used in micromobility. Classic methods can find it hard to tell if a change comes from a genuine blockage or from small natural movements nearby. This challenge motivates the exploration of machine learning-based solutions that can intelligently analyze signal patterns and provide reliable blockage detection. This thesis addresses the following research questions:

1. Can a machine learning-based model help differentiate between dynamic human body blockage and UE micromobility in high-frequency wireless systems like mmWave and sub-THz?

2. If so, what kind of performance such as accuracy and false detection rates can be expect from different machine learning algorithms?

2 Experimental Setup and Measurement Procedures

We are presenting the measurement campaigns conducted to capture the phenomena of blockage and micromobility, both of which are critical in understanding impairments in the system. The data collected has been carefully arranged to reflect a wide range of circumstances and challenges that are encountered in actual environments, as the measurement campaigns have been carefully organized to replicate real-world situations. Focused on accurately capturing their temporal and spectral characteristics, these campaigns documented signal reflections, oscillations, and interruptions caused by obstacles and micromobility events.

Following the data collection process, we outline the procedure for generating SRP (Signal Received Power) time series that incorporate both types of impairments. In order to guarantee that the data is appropriate for further analysis, this approach entails significant stages of preparation such signal normalization, noise reduction, and segmentation. In order to capture the distinct temporal impressions and oscillatory patterns of both blocking and micromobility phenomena, the SRP time series was built.

2.1 Blockage Detection and Measurement Setups

We performed two separate measurement studies to measure the attenuation effects of human body blockage in the THz band independently [1]. The measurement

Table 2.1 *Basic statistical characteristics for BS and UE height 1.65 m*

BS-UE distance	**3 m**	**5 m**	**7 m**
Mean attenuation (dB)	13.87	12.16	7.29
STD of attenuation (dB)	1.18	0.42	0.21
Mean rise time (ms)	59.26	85.73	102.51
STD of rise time (ms)	36.72	44.51	30.93
Mean fall time (ms)	62.39	79.17	95.57
STD of fall time (ms)	38.92	46.89	29.34
Mean blockage time (ms)	383.72	376.12	361.92
STD of blockage time (ms)	32.17	47.31	36.13
STD of signal in blockage state	0.44	0.21	0.68
STD of signal in non-blockage state	0.027	0.017	0.029

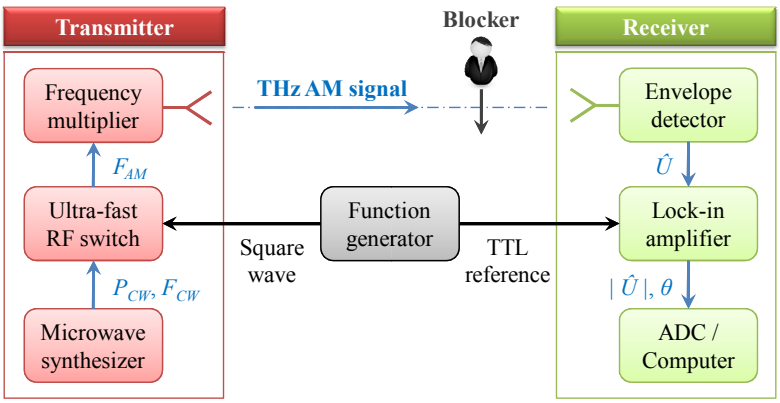

Figure 2.1 *Schematic diagram of the blockage measurement setup [1].*

system used THz transmitter (Tx) and receiver (Rx) equipment running at 156 GHz with 90 mW output power. The measurement apparatus used pyramidal horn antennas with an operating HPBW of 10 ° and an antenna gain of 25 dB. The measurement area consisted of an empty hall measuring 7.5 m long and 3 m high. The channel sampling resolution of 50 µs appeared in both studies as did the amplifier time constant which stayed at 30 µs. The main difference between experiments concerns the measurement hall dimension which extends to 4.5 m, yet another set-up operates within 2.4 m but this difference does not substantially affect measurement outcomes [35]. Measurements were made in three Tx-to-Rx distance settings that ranged from 3 m up to 5 m and 7 m. A human blocker traversed the direct sight path at a velocity of 3.5 km/h while using the entire length from 3 to 7 meters. This represented practical blockage situations. Patent design and deployment parameters included two antenna height implementations:

$h = 1.35$ **m:** Simulating LoS blockage by a person's chest.

$h = 1.65$ **m:** Simulating LoS blockage by a person's head.

The placement of blockers involved different positions to assess multiple blockage situations in the test area.

- For $x = 7$ m: $d = 1.5$ m, 2.5 m, 5.5 m.
- For $x = 5$ m: $d = 1.5$ m, 2.5 m.
- For $x = 3$ m: $d = 1.5$ m.

The study was conducted thirty times for each configuration to ensure statistical reliability. The resulting data set provided detailed insight into how blockage affects communication links across various distances and heights. While Table 3.1 summarizes the key statistical features, Figures 3.2 illustrate the typical behavior of the blockage event.

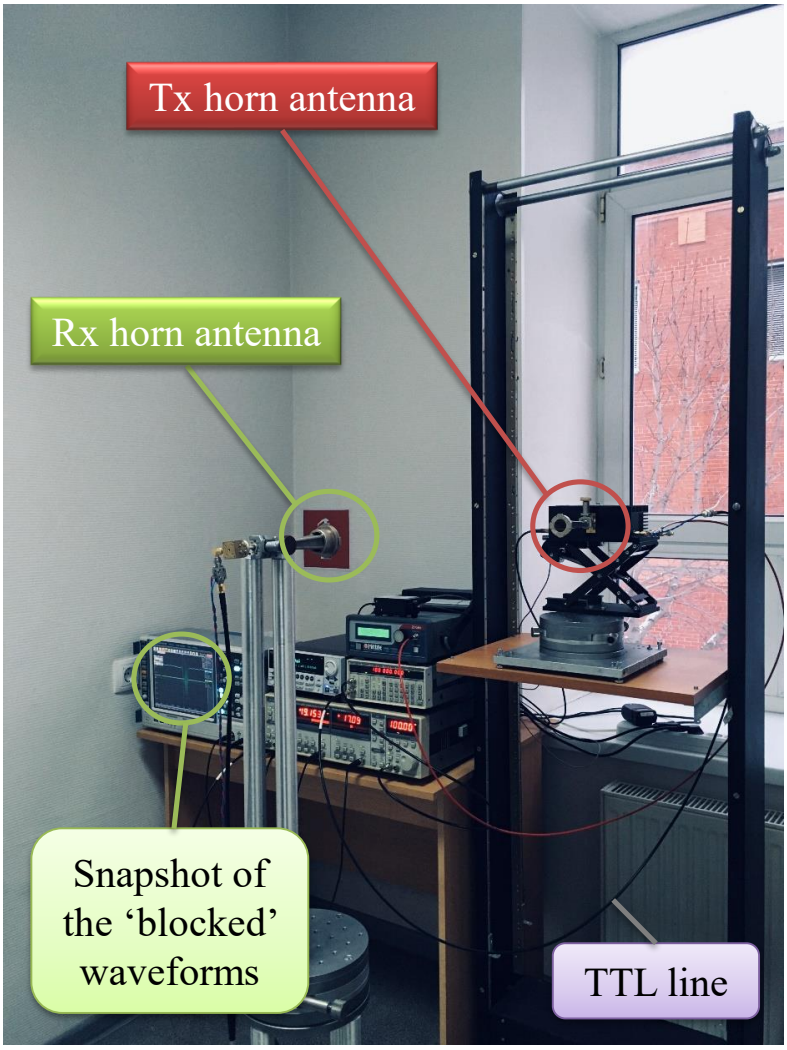

Figure 2.2 *Illustration of the experimental setup [1].*

2.2 Micromobility Detection and Measurement Setups

The micromobility measurement campaign focused on four application scenarios: Racing game, Phone call, VR viewing, Video streaming. The mobility patterns of users were first emulated using an approach described in [36].Using a controlled experimental setting to capture exact movement patterns, the method outlined in the cited article was used to first simulate the mobility patterns of users. To follow the motions of user equipment, the measurement campaign used a Nikon D3100 camera in video recording mode at 1280x720 resolution and 30 frames per second. To represent the center of the THz beam's half-power beamwidth (HPBW), a laser pointer mounted on mobile devices with precise parameters was used. For tracking purposes, the laser beam was projected onto a flat wall surface.

In order to improve contrast for data processing, the experimental setup was carried out in a dark room setting with a 2-meter gap between the user equipment and

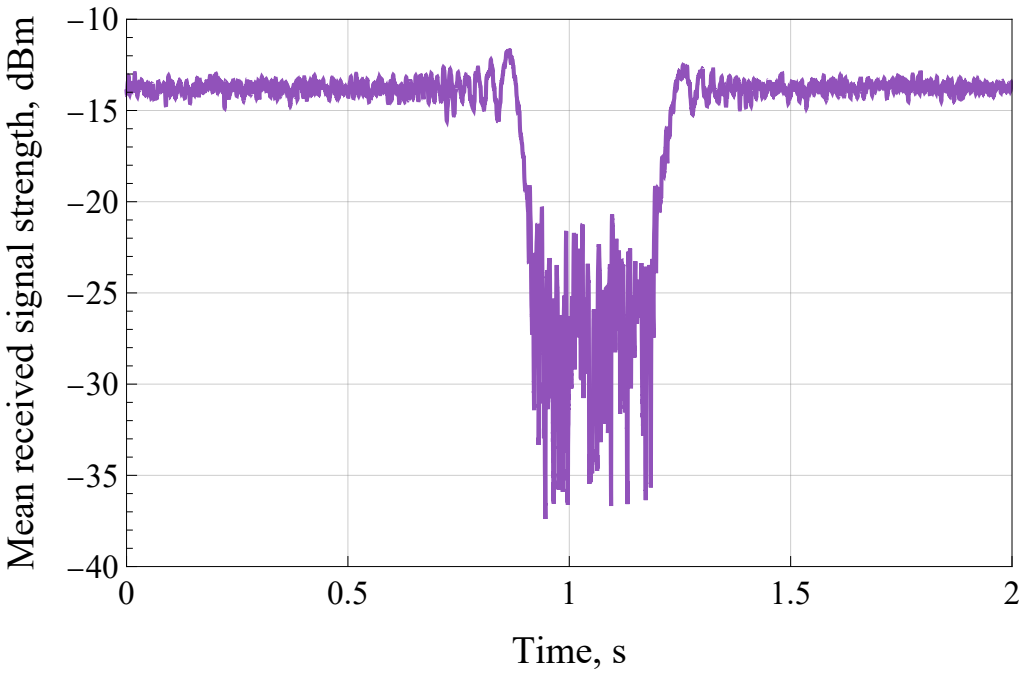

Figure 2.3 *Typical signal behavior during the blockage event.*

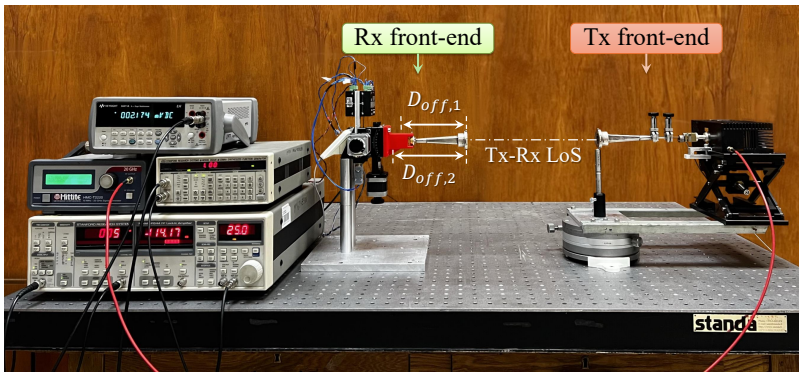

Figure 2.4 *Illustration of the experimental setup for micromobility*

the observation wall. The observed area was 1.5 x 2.5 meters. The laser pointer was positioned perpendicular to the horizontal axis of the smartphone for applications such as video viewing, racing games, and phone calls, and parallel to the floor on the VR console for VR viewing. Each application scenario reflected unique micro-mobility features: VR viewing recorded head movement patterns during 3D movie viewing, the racing game application generated semi-regular movement patterns as users controlled vehicle positioning through built-in motion sensors, and video viewing and phone calling applications produced natural hand tremor patterns as users tried to maintain stationary positions without conscious stabilization efforts.

Ten separate tests, each lasting 10 seconds and producing a 30-frames-per-second video clip, were used as the basis for the statistical analysis. This produced over 3,300 sample points per application trace. Since major directional changes were

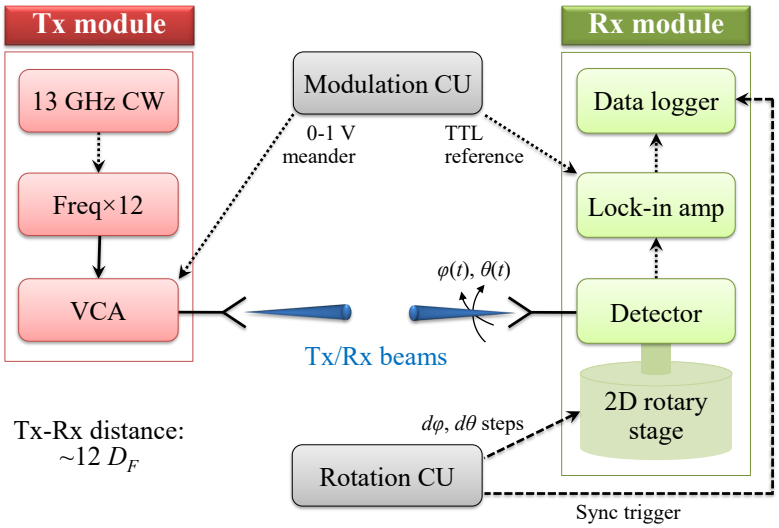

Figure 2.5 *Schematic diagram of the experimental setup for micromobility*

Table 2.2 *Micromobility statistics for different applications*

S_{th} (dB)	Racing	Calling	VR
3	70.24	198.242	175.8177
5	87.2753	255.8403	261.9927
7	92.0423	471.38	295.9297
10	96.0087	599.1333	316.365
15	114.8423	1013.0633	341.2

unlikely to occur within this timeframe, it was found that the 33-millisecond time resolution between frames was adequate for capturing changes in the trajectory of user equipment. This allowed for possible interpolation to higher temporal resolutions using linear or more intricate techniques. A 2D Markov chain system was designed to simulate user movements between distinct states while taking into account velocity-shift patterns and motion axis relation effects.

A static transmitter (Tx) acted as a base station (BS) emulator, while a mobile receiver (Rx) provided user device simulation. A high-directivity horn antenna powered the 156 GHz Tx to produce 44 mW of output power.see Fig. 2.4 and Fig. 2.5 The Rx receiver operated 400 cm from the Tx transmitter before initial alignment to achieve maximum beam precision. The Rx movement system used goniometers that provided precise speed control up to 80°/s for horizontal (yaw) and vertical (pitch) axis movement [37]. The production of control traces was required using time series data from the Markov model. The antenna movement states were recorded with 1 for step movements, while 0 indicated stationary states in the data traces. The channel measurement sampling resolution operated at $\Delta = 50$ μs.

A study evaluated the duration for the received signal strength to descend past levels of 3, 5, 7, 10, and 15 dB. The beam alignment was precise at t = 0 because the signal strength measured 15 dBm. The highest rate of movements occurred in racing games that created regular beam alignment disruptions. The directional movements in virtual reality applications occurred at a moderate pace while occurring frequently. Video calls and phone usage experienced slow-moving movement patterns that generated stable connections. While 2.2 provides the primary statistical properties, Fig. 3.1 displays the usual micromobility behavior for the various investigated applications.

3 Proposed Algorithms

In this chapter, we will take a closer look at the joint time series data, which involves both blockage and micromobility events. this is really important because it is the main base of out detection mathod of blockage. we are explaining here how these events are captured and how they interact over time.

Next, we will give an idea of the machine learning algorithns we have considered for this task. Each one has has its own set of features and capabilities, and discussion why we think they might be a good fit for detecting blockages. To achieve the best results we need to select the optimal algorithm before optimizing its settings. The processing of data and accurate blockage event detection by the algorithm will be explained through successive steps.

3.1 Joint Time Series

Micromobility and obstruction effects on SRP cannot be captured simultaneously by thorough measurements due to the current limits of sub-THz experimental equipment. Despite this technical limitation, by combining isolated data of these distinct processes, researchers can use a superposition methodology to generate realistic SRP profiles. By carefully adjusting the signal intensity patterns obtained to account for interruptions brought on by required beamtracking techniques, this reconstruction method combines blockage and micromobility processes. The methodology sets parameters for forecasting future blockage events and starts with system initialisation at t = 0 in an unblocked state, just after beam alignment.

In order to forecast blockage frequency in dynamic situations, this temporal model takes into consideration blocker density, movement velocity, and physical dimensions. Their study showed that human mobility patterns in cities produce regular blockage intervals that are statistically accurate to describe mathematically. The time interval until blockage occurs follows an exponential distribution, with the mean calculated using the formula derived by [38]:

$$\lambda_B = \frac{2\rho_B v_B r_B}{\pi}, \tag{3.1}$$

where λ_B represents the blockage rate, ρ_B is the density of blockers in the environment, v_B denotes the average blocker velocity, and r_B corresponds to the effective blocker radius. This equation provides a mathematical foundation for predicting blockage frequency in dynamic environments.

Using least-mean-squares fitting techniques on empirical data, application-specific

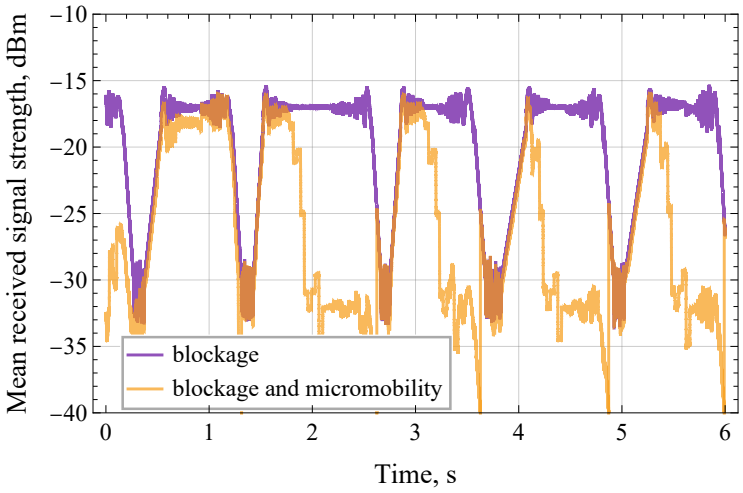

(a) On demand beamtracking

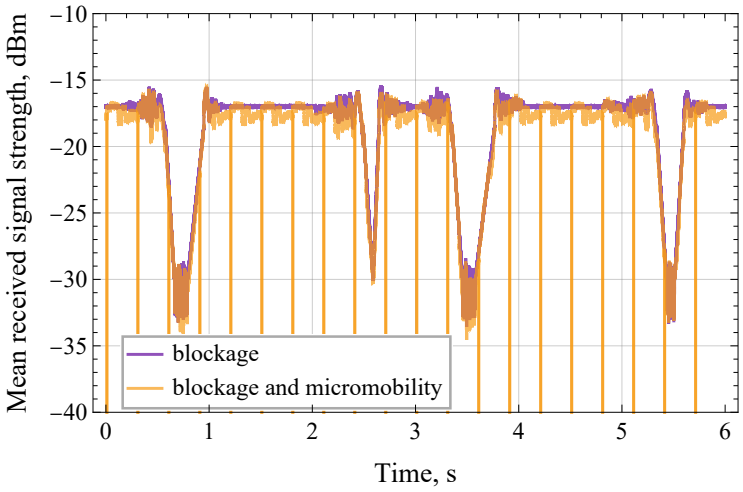

(b) Regular beamtracking

Figure 3.1 *Signal behavior during blockage and micromobility for VR application.*

signal degradation patterns are identified for the micromobility component. Depending on the specific mobility characteristics of the use case, this method enables accurate modeling of the impacts of gradual misalignment of the beam. Realistic signal received power (SRP) behavior under micromobility settings is then produced by combining the obtained trend with regularly distributed signal strength changes. It is possible to characterize the angular deviation $\theta(t)$ for the micromobility component as a random process with time-dependent variance [39].

$$\theta(t) \sim \mathcal{N}(0, \sigma_\theta^2(t)). \tag{3.2}$$

The procedure resets after predefined intervals when regular beam-tracking tactics are implemented, taking into account the beam-search delay factor. The hierarchical beam searching technique introduces a delay penalty proportional to the number of

antenna components in the base station and user equipment, multiplied by the array switching latency, as illustrated in [39]. The signal strength temporarily decreases to outage levels during these realignment times.

The temporal features of blocking occurrences follow certain statistical distributions, which can be precisely modeled using truncated normal distributions, as confirmed in [38]. The superposition technique accurately represents the frequency and length of blockage episodes by integrating these well-established models.

This reconstruction process maintains the essential features shown in the empirical data, although it just approximates rather than precisely replicates the real-world SRP behavior. For creating and assessing performance improvements for upcoming sub-THz communication systems in the 6G era, this makes it an invaluable tool.

3.2 Machine-Learning Classification

Multiconnectivity and other system-level blockage avoidance techniques require the ability to identify blockage events before they happen. Recent strategies have used machine learning methods in the time domain to achieve this [35]. Identifying patterns within noisy signals caused by user equipment (UE) micromobility, particularly when devices are held in users' hands, requires more sophisticated analytical frameworks. To address this challenge, we evaluated multiple categories of machine learning (ML) algorithms specifically designed for effective pattern recognition in complex signal environments. These approaches offer improved capabilities for detecting and interpreting signal variations amid micromobility-induced noise that characterizes real-world usage scenarios.

3.2.1 Random Forest

Random forests are an ensemble machine learning algorithm that combines multiple decision trees. Each tree independently classifies the data and casts a vote for the most frequent class. The final classification result is determined by aggregating these votes. Random forests offer high classification accuracy, are robust to outliers and noise, and do not suffer from overfitting. As a result, they have become one of the most widely used techniques in data mining research. [40]

A random forest is a classifier composed of multiple tree-structured models, represented as $\{h_k(x, Z_k)\}_{k=1}^{K}$, where each Z_k is an independently and identically distributed (i.i.d.) random variable. Each tree contributes a single vote for the most frequently occurring class at a given input x. This definition illustrates that a random forest consists of multiple decision trees. In Breiman's random forest model, each tree is constructed using a training dataset and a corresponding random variable Z_k. These random variables are independent and identically distributed

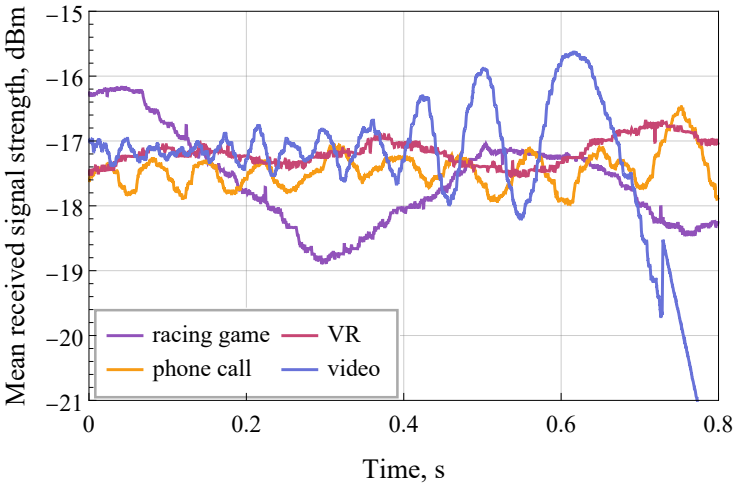

(a) Oscillation

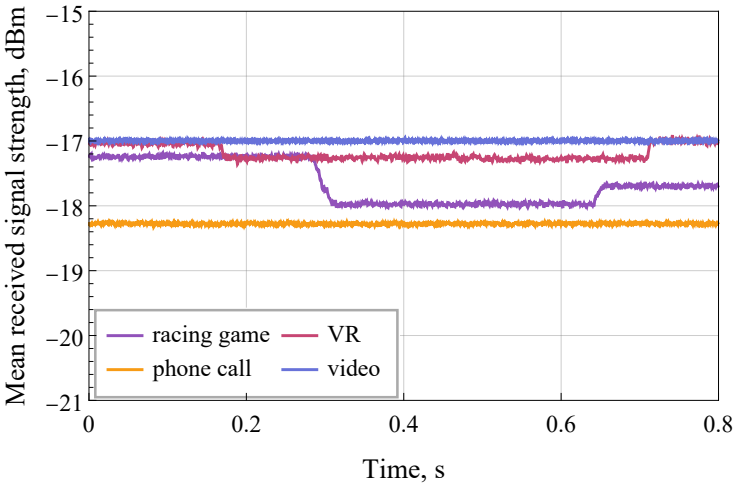

(b) Non-blockage

Figure 3.2 *Signal behavior during oscillation and non-blockage.*

across different trees, leading to a classifier $h_k(x, Z_k)$, where x represents the input feature vector.

After running the model K times, a sequence of classifiers $\{h_1(x), h_2(x), \ldots, h_K(x)\}$ is obtained. These classifiers collectively form an ensemble system and the final classification result is determined by a majority voting mechanism. The decision function is given by:

$$H(x) = \arg\max_{Y} \sum_{i=1}^{K} I(h_i(x) = Y), \tag{3.3}$$

where $H(x)$ represents the final classification model, h_i is an individual decision tree, Y is the output variable, and $I(\cdot)$ is an indicator function. For any given input, each

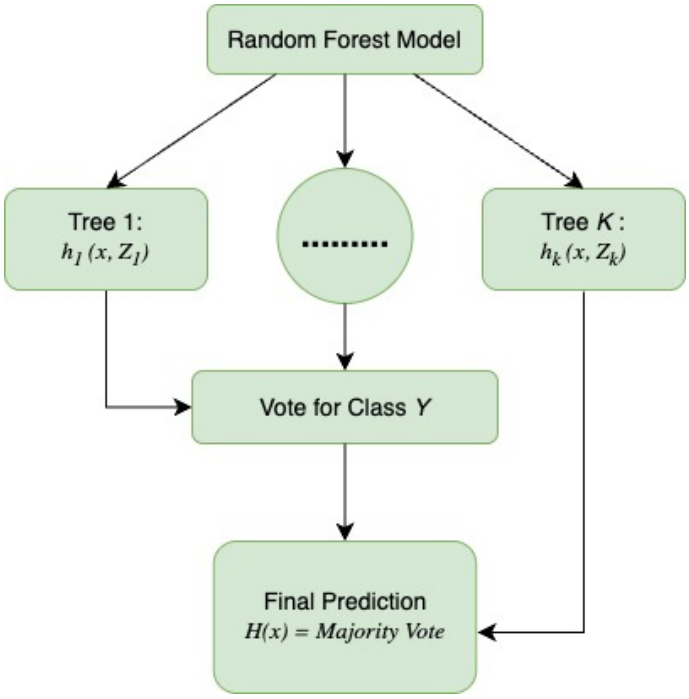

Figure 3.3 *Random Forest Classifier*

tree in the ensemble votes to determine the most suitable classification outcome.

3.2.2 Decision Tree

Decision tree classifiers are widely recognized for their ability to provide a clear representation of performance outcomes. Their high accuracy, optimized splitting criteria, and advanced pruning techniques make them essential in various data classification tasks. These classifiers use distinct datasets to train models from large data pools like us, which in turn influences the accuracy of the test set. However, decision trees face challenges related to robustness, scalability, and height optimization. Despite these concerns, they stand out from other classification methods by generating a well-structured set of rules that are both efficient and easy to interpret. [41] In decision tree classification, the attribute that provides the highest information gain is typically chosen for splitting. Information gain is determined by computing the difference between the initial entropy and the entropy after the split. Entropy, which ranges from 0 to 1, measures the level of uncertainty or impurity in the data. It is calculated using the following formula:

$$H(Y|X) = \sum_{x \in X} P(x) H(Y|X = x). \tag{3.4}$$

Consider a dataset S consisting of s samples, where the target variable has m distinct categories $(C_1, C_2, C_3, ..., C_m)$. Let S_i represent the number of samples belonging to

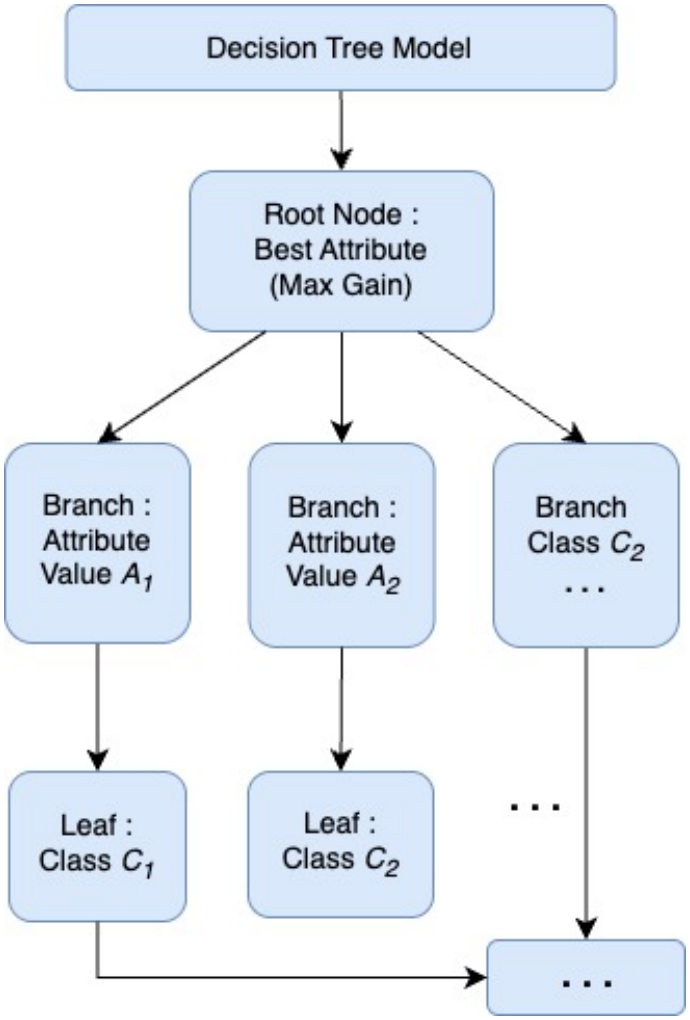

Figure 3.4 *Decision Tree Classifier*

category C_i. The total information entropy of the dataset is given by:

$$I(S_1, S_2, ..., S_m) = -\sum_{i=1}^{m} P_i \log_2 P_i, \tag{3.5}$$

where P_i denotes the probability of a sample belonging to category C_i, which can be estimated as:

$$P_i = \frac{S_i}{S}, \tag{3.6}$$

Now, assume that an attribute A has K distinct values $\{A_1, A_2, ..., A_K\}$, leading to the division of dataset S into K subsets $\{S_1, S_2, ..., S_K\}$. Each subset S_j contains the samples where attribute A has value A_j. If attribute A is chosen for splitting, the new subsets become child nodes of the decision tree. Let S_{ij} be the number of samples in subset S_j that belong to category C_i. The entropy of the dataset after splitting on attribute A is given by:

$$E(A) = \sum_{j=1}^{K} \frac{|S_j|}{|S|} I(S_{j1}, S_{j2}, ..., S_{jm}). \tag{3.7}$$

Finally, the information gain obtained by splitting on attribute A is calculated as:

$$Gain(A) = I(S_1, S_2, ..., S_m) - E(A). \tag{3.8}$$

This value indicates the reduction in uncertainty or impurity achieved by partitioning the dataset based on attribute A. The attribute with the highest information gain is preferred for making splits in the decision tree. [42]

3.2.3 XGBoost

XGBoost is a gradient boosting method that incorporates regularization, allowing the adjustment of variable weights. This feature sets it apart from other boosting techniques, as it helps mitigate overfitting more effectively than traditional Gradient Boosting Machines (GBM) that lack regularization. By penalizing variable importance in high-dimensional datasets, XGBoost facilitates variable selection.

Regularization reduces overfitting without compromising predictive performance, enabling the model to generalize well to unseen data. The final model is formed by aggregating all the individual trees, with the prediction output defined as:

$$Z_i = G(X_i) = \sum_{j=1}^{K} g_k(X_i), \tag{3.9}$$

where X_i represents the input features, and $g_k(X_i)$ is the output function of each tree. Like many machine learning algorithms, XGBoost relies on hyperparameter tuning to optimize performance. Machine learning is an iterative process in which model accuracy is progressively enhanced. During each iteration, specific parameters are adjusted to refine performance. However, these optimal parameter values cannot be directly inferred from data and must be fine-tuned separately for each predictive modeling task. Hyperparameter tuning, therefore, identifies the best parameter configuration to maximize model accuracy. [43]

3.2.4 Autoencoder

Autoencoders (AEs) a subclass of neural networks that learn significant representations of input data through unsupervised reconstruction tasks. As illustrated in Fig. 3.6,these models have a symmetric encoder-decoder architecture with an output layer that reflects the dimensionality of the input layer. The main goal is to encode the input patterns into low-dimensional latent representations and then decode them

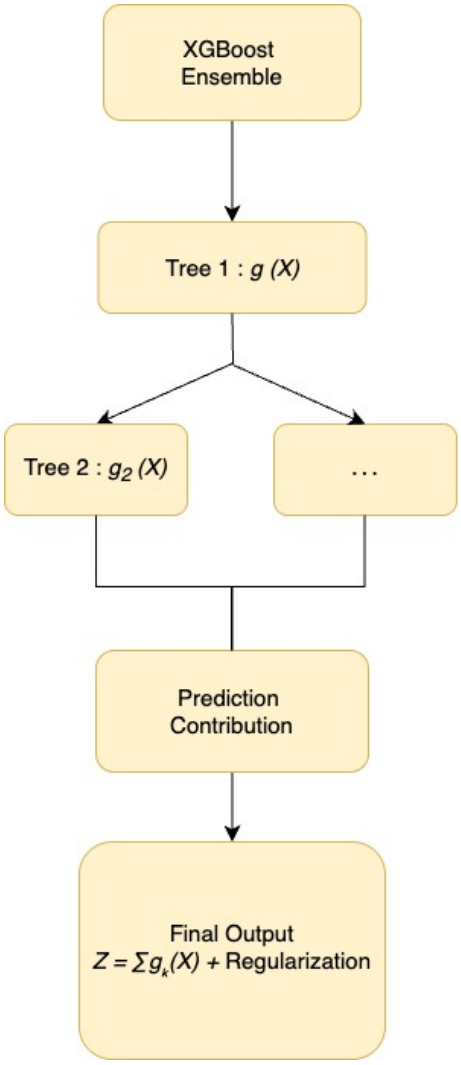

Figure 3.5 *XGBoost Model*

to obtain the original data with low information loss. This built-in feature renders AEs to be very suitable for anomaly detection in high-dimensional spaces, as it is possible to learn low-dimensional encodings of normal data, with abnormal data resulting in high reconstruction error. We used autoencoder-based anomaly detection compress our dataset into a latent space with a smaller dimension than the original data and the differences between the restored and original data compared. We used normal data to train an autoencoder and tracking the reconstruction error, we identified situations in which the error exceeds a predetermined threshold. When it occurs, we are aware that we have discovered an anomaly.

The implemented AE consists of two functionally distinct modules: First one is encoder network which transforms input vectors $\boldsymbol{x} \in \mathbb{R}^{1500}$ into compressed latent representations $\boldsymbol{g} \in \mathbb{R}^{32}$ through non-linear projection:

$$g = \sigma_{\text{enc}}(W_e x + b_e), \tag{3.10}$$

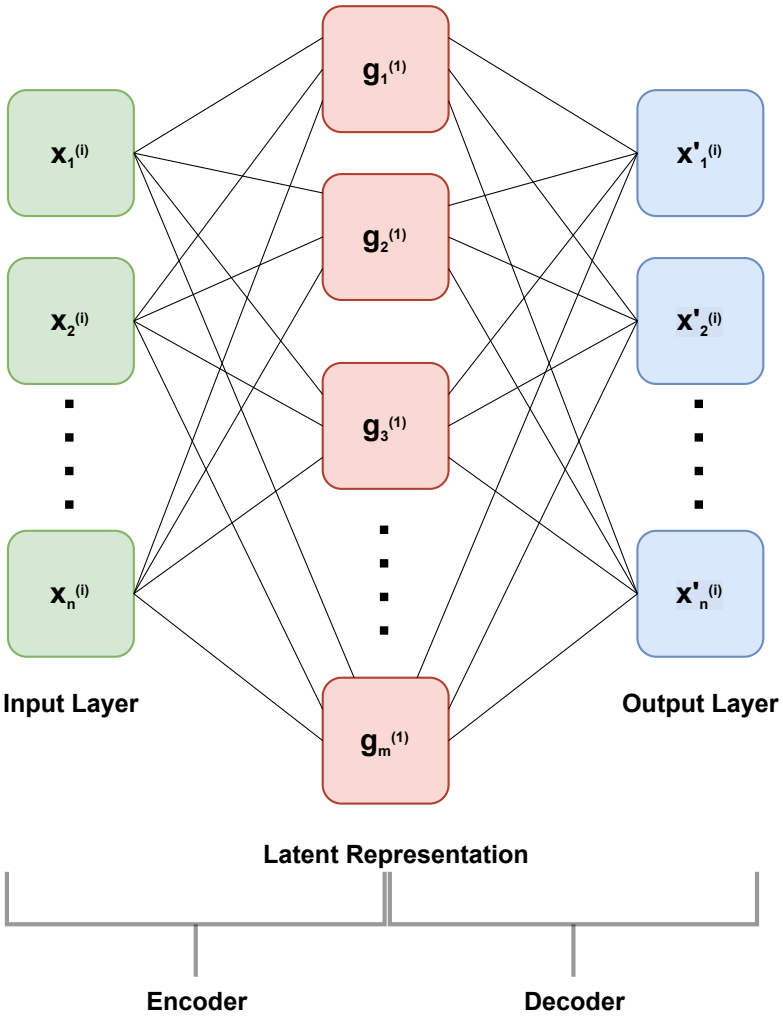

Figure 3.6 *An architechture of autoencoder*

where $W_e \in \mathbb{R}^{32\times1500}$ denotes the encoder weight matrix and $b_e \in \mathbb{R}^{32}$ the bias vector. σ_{enc} the rectified linear unit (ReLU) activation introduces sparsity while maintaining gradient stability during backpropagation. Then reconstructs the original input space $x' \in \mathbb{R}^{1500}$ from latent codes by inverse mapping:

$$x' = \sigma_{\text{dec}}(W_d g + b_d), \tag{3.11}$$

employing a dense layer activated by sigmoids with parameters $W_d \in \mathbb{R}^{1500\times32}$, $b_d \in \mathbb{R}^{1500}$. The activation of sigmoids restricts the output values to $[0, 1]$, facilitating a probabilistic interpretation of the fidelity of reconstruction. The severe reduction in dimensionality (1500 32 units) in the bottleneck layer forces the network to remove redundant features, but retain the important features of normal opera-

tional data. This paradigm of compressing, decomposing, and compoitioning allows the model to discover salient data manifold and to remain sensitive to distribution shifts caused by anomalies. Calculating whether the reconstruction loss exceeds a predetermined threshold allows anomalies or non-blockage to be identified. In this paper, the mean error for the training set's normal instances is calculated, and if the reconstruction error exceeds the training set's standard deviation, subsequent examples are categorized as abnormal or non blockage [44]. In unsupervised training, the autoencoder (AE) optimizes parameters, $\theta = \{W_e, b_e, W_d, b_d\}$ for minimizing the reconstruction error (RE) between input x and output x':

$$\mathcal{L}(\theta) = \|x - x'\|^2. \tag{3.12}$$

The training process iteratively adjusts weights in the network via backpropagation until the model converges to a point at which it can stably reconstruct normal patterns [45]. Most importantly, the training dataset consists of solely nominal operational data, allowing the AE to learn specialized reconstruction abilities for in-distribution samples. During inference, anomalies are detected when reconstruction errors exceed statistically derived thresholds. We compute the threshold T from training-set reconstruction losses r:

$$T = \mu_r + \sigma_r, \tag{3.13}$$

where μ_r and σ_r are the average and the standard deviation of losses throughout training, respectively. Let us assume T represents the 84th percentile using normal samples, approximating a quasi-Gaussian distribution error, derived from the 68-95-99.7 empirical rule. Samples satisfying $r_{\text{test}} \leq T$ are classified as normal oscillations, while $r_{\text{test}} > T$ indicates abnormal/non-blockage states. Mean Absolute Error (MAE) measures pixel-wise differences between input x and reconstruction x':

$$\text{MAE}(x, x') = \frac{1}{n} \sum_{i=1}^{n} |x_i - x'_i|, \tag{3.14}$$

where $n = 1500$ is related to the input dimension. MAE was chosen instead of Mean Squared Error (MSE) since it linearly penalizes errors, therefore reducing the over-sensitivity of the metric in response to outlier pixels that can conceal subtle anomalies. In this paper, we uses sigmoid function as the activation function. By determining the type and magnitude of signals flowing in the neural architecture that are connected through activation functions, activation functions connect the sequential layers in a neural network. These functions introduce non-linear transforms, basically acting as dynamic gates to block out irrelevant features while enhancing salient ones [46]. Such selective filtering allows neural networks to function

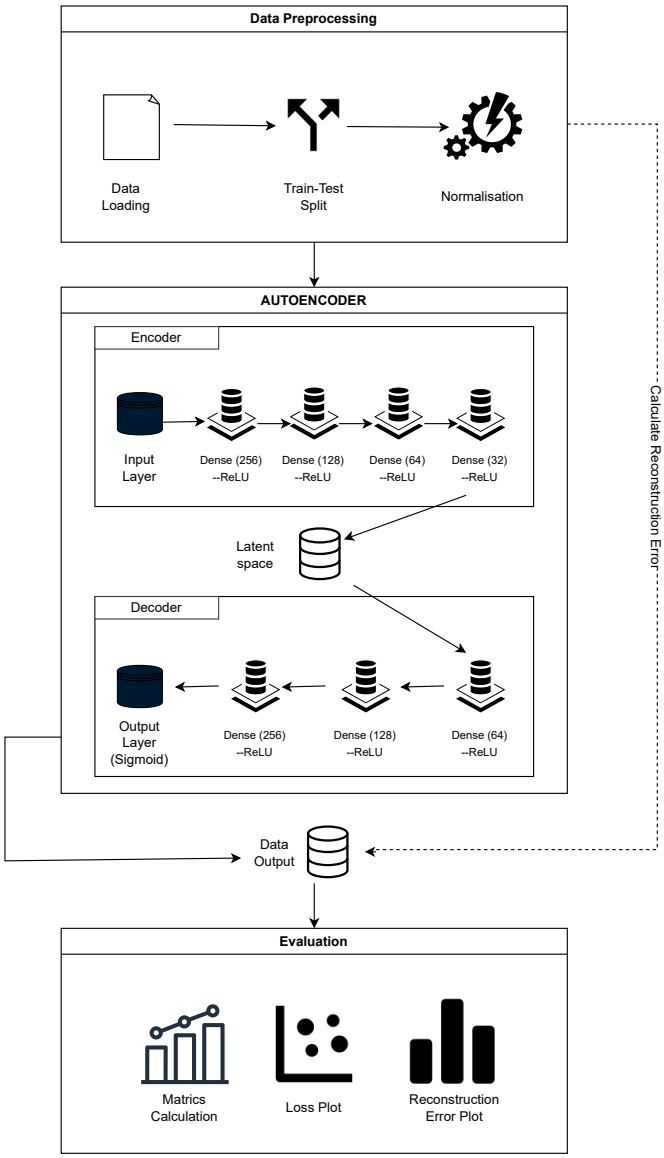

Figure 3.7 *Autoencoder Model*

in the space of complex representations rather than simplistic linear approximations. Some of the most used activation functions are Sigmoid function, Hyperbolic Tangent function (tanh), and Rectified Linear units (ReLu). In this paper we used sigmoid and ReLu function in the encoder and decoder layers. Sigmoid function

$$f(a) = \frac{1}{1 + e^{-a}}, \tag{3.15}$$

where $a \in \mathbb{R}$ shown by the curve of sigmoid function visualization Fig. 3.8(a). The

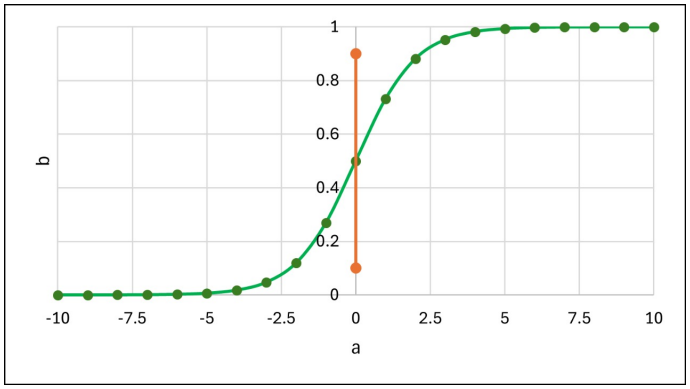

(a) Sigmoid Function

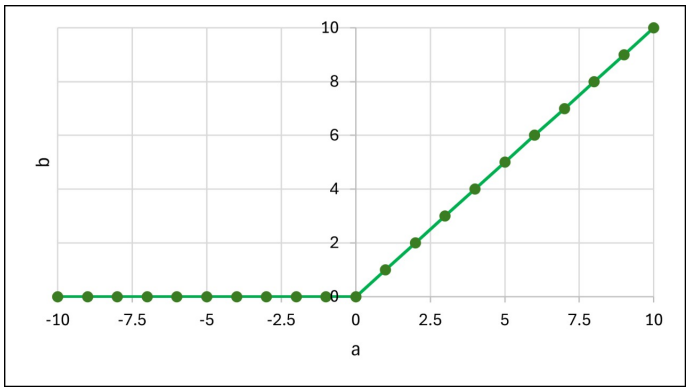

(b) Rectified Linear unit function

Figure 3.8 *For sigmoid function the values are bounded between 0 and 1.For ReLu values are between 0 and infinity*

range of the value of this function is between 0 and 1 and 0 centered, as shown in the orange vertical line. Additionally, ReLU has been widely employed, particularly in conjunction with convolutional neural networks. The formula for ReLU is:

$$f(a) = \max(0, a), \tag{3.16}$$

which accepts the highest value between 0 and its input value. Fig. 3.8(b) vividly illustrates the ReLU activation function's feature, which only passes positive values.

3.2.5 LSTM

Long Short-Term Memory (LSTM) networks are a specialized class of Recurrent Neural Networks (RNNs) designed to handle long-range temporal dependencies in sequential data. Their architecture includes memory cells and input, output, and forget gates that allow the network to selectively remember or forget information over time. This makes LSTMs particularly effective for modeling complex, time-dependent processes without requiring predefined time windows. [47]

We used LSTM networks to separate micromobility patterns and blockage events.

Regular device movements along with environmental changes produce micromobility patterns through small consistent signal alterations, yet blockage events occur as sudden long-lasting disruptions because of physical barriers in the signal path. LSTM trains exclusively with normal sequences during the development phase of anomaly detection. Through training, the model analyzes typical sequence patterns in these data, which results in forecasting accuracy. The system detects anomalies by monitoring prediction mistakes that occur after the learned pattern deviates from its expected course. Let the multivariate time series be denoted as:

$$\mathbf{x}_t \in \mathbb{R}^d, \quad t = 1, 2, \ldots, T, \tag{3.17}$$

where $\mathbf{x}_t$ represents the sensor readings at time t, and d is the number of input features (e.g., signal strength, angle, distance). The LSTM network is trained to predict the next h time steps using all previous observations up to time t:

$$\hat{\mathbf{x}}_{t+1:t+h} = \text{LSTM}(\mathbf{x}_{1:t}), \tag{3.18}$$

After training, the prediction error for each point is calculated as the squared difference between the predicted and actual future values:

$$\text{AnomalyScore}_t = \left\| \mathbf{x}_{t+1:t+h} - \hat{\mathbf{x}}_{t+1:t+h} \right\|^2. \tag{3.19}$$

A threshold is then applied to the anomaly score to classify the behavior at each time point. If the score exceeds a threshold θ, the event is considered anomalous, likely indicating a blockage. [47] To improve robustness, the prediction errors across multiple future steps are modeled as a multivariate Gaussian distribution. The likelihood of an observation being "normal" is assessed by evaluating how probable its error vector is under this distribution. Low likelihood values suggest a departure from the learned micromobility behavior. This statistical modeling allows the system to tolerate occasional small prediction errors due to noise while still being sensitive to sustained and structured deviations like those caused by blockages. We wanted to show that the LSTM-based anomaly detection approach offers several key advantages in distinguishing between micromobility and blockage events. First, it eliminates the need for manually defined time windows or handcrafted features, as the LSTM network automatically learns both short- and long-term temporal dependencies directly from the data. This makes the model flexible and adaptable to varying signal behaviors. Second, the approach is particularly effective in scenarios where anomalous data is scarce, since it is trained solely on normal sequences, making it well-suited for real-world applications where blockages are rare or hard to label. Lastly, by statistically modeling the prediction error distribution, the method

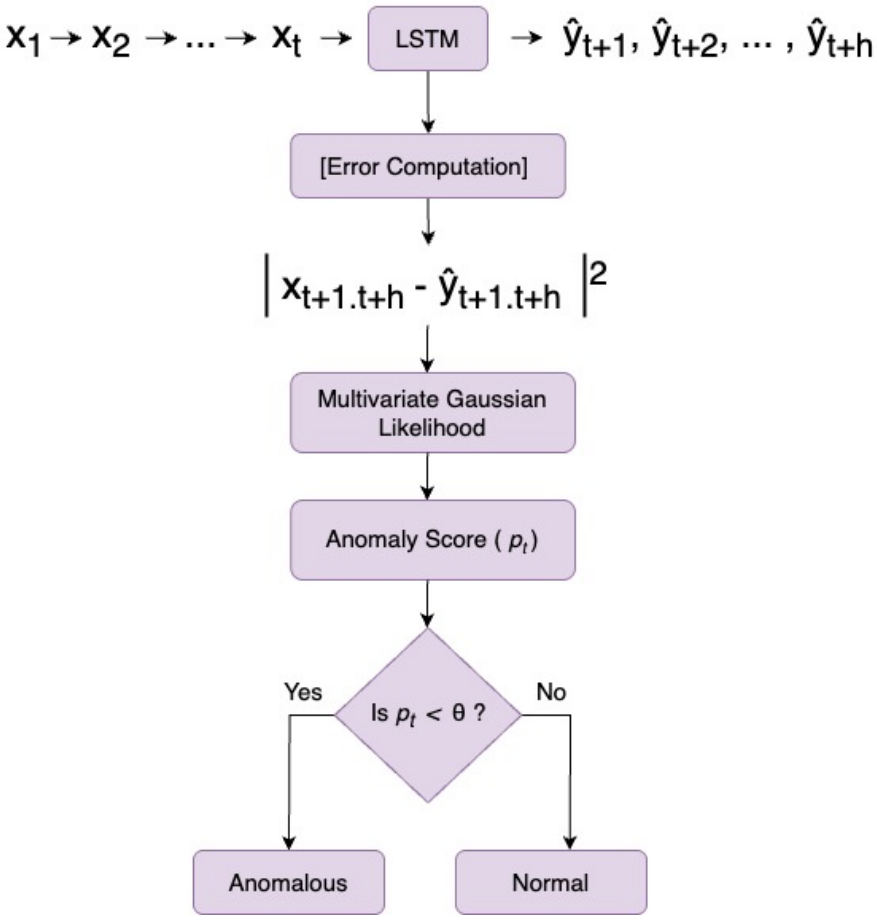

Figure 3.9 *A representation of LSTM model*

achieves robustness to noise while maintaining sensitivity to abrupt or sustained deviations, such as those introduced by physical obstructions in the environment. This balance between adaptability and sensitivity is crucial for accurate and real-time detection in dynamic systems.

4 Numerical Analysis

In this section we generate numerical results that maintain consistency and quality throughout the investigation. The defined performance metrics allow an evaluation of the model through its ability to measure both prediction accuracy and impairment detection performance. The research study analyzes two different conditions: Scenario A sets the baseline without micromobility, whereas Scenario B evaluates the system during its operation with micromobility enabled. The analytical combination serves to establish a complete understanding regarding the model's operation across multiple conditions.

4.1 Data Acquisition and Preprocessing

The collected data includes two signal trace types: one consisting only of blockage events and the other containing blockage and micro mobility patterns. The main intent of this research project involves building a machine learning system that can recognize time-domain oscillations with accuracy. Supervised learning processing involved segmenting the traces through the extraction of representative windows from both types during times with either oscillatory motion or without blockage occurrences. The selected time sequences contain 1500 continuous timesteps which provides an adequate window for detecting pattern dynamics.

The labeling process involved binary classification where oscillation segments obtained the value zero while non-blockage segments received the value one. The labeling system creates a straightforward supervised learning format for classification tasks. The analysis excluded all preprocessing steps including filtering and normalization for the raw signal dataset. We made this arrangement on purpose so that the model could absorb information from intrinsic raw measurement attributes including amplitude fluctuations, periodic shapes and transitory variations. Keeping the natural signal properties intact serves the model well as it enables it to detect hidden patterns that may otherwise disappear during normalization steps.

The system design adopts end-to-end learning approaches that shift feature extraction responsibility from human operators to the automated model architecture. The range of blockage signatures from simple to complex creates an effective learning basis for developing models that handle realistic communication signal patterns.

4.2 Performance Metrics

The evaluated metrics to assess the proposed algorithms comprise precision, precision and recall. The evaluation of classification tasks relies heavily on accuracy

since it represents their fundamental evaluation benchmark. A model's overall performance can be evaluated through this metric which measures the proportion of correctly predicted items compared to the complete dataset.

The evaluation of balanced datasets benefits greatly from accuracy measurements because class samples remain equal in number. The accuracy measure provides reliable performance assessment in our data set because it follows the requirement of balanced classes. The mathematical formulation for accuracy, denoted as $\mathcal{A}$, is given by:

$$\mathcal{A} = \frac{t}{T}, \tag{4.1}$$

where, t represents the number of correctly predicted instances, T denotes the total number of instances in the evaluation set. This metric provides a straightforward interpretation: a higher value of $\mathcal{A}$ indicates that the model is more successful in predicting the correct class labels. The most straightforward and popular criterion for assessing a classifier's performance is accuracy. However, accuracy isn't always a useful indicator, particularly when there are imbalances in the data. The fundamental issue is that we can only attain high accuracy when the negative class is dominant if we forecast negative most of the time. Therefore, it is possible that the negative class is (much) more likely even when a highly accurate classifier generates a positive prediction. These circumstances are defined by a precision of 50% or less. In a lot of applications, this is really undesirable. Having precision and recall as performance metrics allows researchers to understand model behavior regarding the minority class data specifically [48]. Precision reveals the rate at which correct positive predictions originate from total positive results given by the model. The measurement holds enormous importance in situations with expensive false positive consequences. An incorrect pulse indication from this algorithm could trigger system procedures that prove unnecessary. The mathematical expression for precision, denoted as $\mathcal{P}$, is defined as:

$$\mathcal{P} = \frac{t_p}{t_p + f_p}, \tag{4.2}$$

where, t_p represents the number of true positive predictions, f_p indicates the number of false positive predictions. In the ideal scenario where the model makes no false positive errors (i.e., $f_p = 0$), the precision reaches its maximum value of 1, indicating perfect reliability in positive predictions. Recall refers to the proportion of true positive instances correctly identified out of all actual positive cases. It is calculated as:

$$\mathcal{R} = \frac{t_p}{t_p + f_n}, \tag{4.3}$$

where t_p denotes the number of true positives and f_n is the number of false negatives.

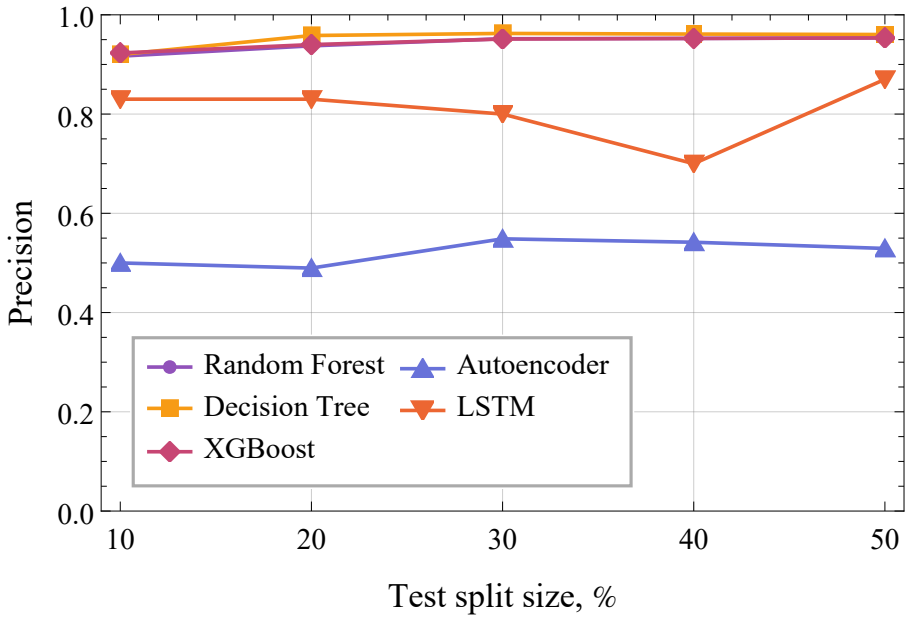

(a) Precision

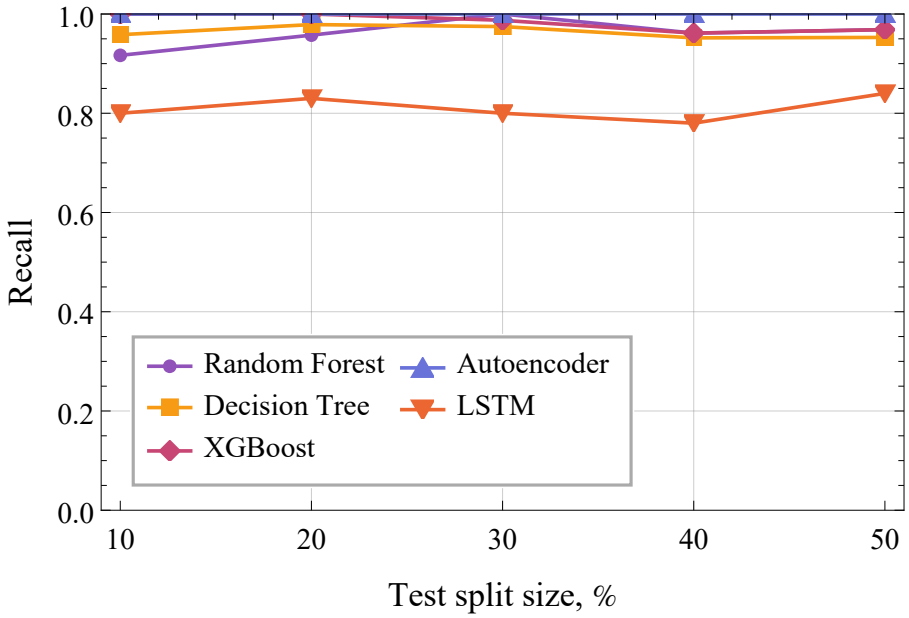

(b) Recall

Figure 4.1 *Precision and recall when detecting blockage without micromobility.*

Similar to precision, recall reaches its maximum value of 1 when no false negatives are present (i.e., $f_n = 0$). A low recall measurement shows that several real oscillation events which signal blockage get identified as non-oscillation. The failure to detect oscillation followed by an outage proves more serious because it stops the system from starting a new association. The UE maintains beam tracking functions with the presently blocked base station so the service outage duration lengthens. The outage duration depends on how long the beam tracking failure timers have been

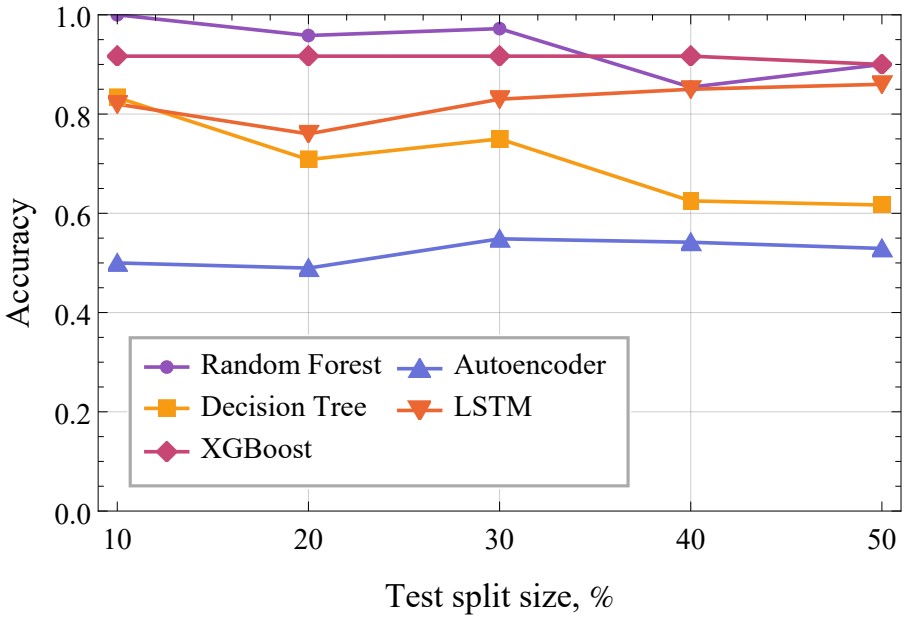

Figure 4.2 *Accuracy when detecting blockage with micromobility.*

activated. [49]

4.3 Scenario A: Absence of Micromobility

A preliminary examination was carried out on signal traces that were only hampered by blocking phenomena, leaving out any disruptions caused by micromobility. Accurately identifying the oscillation period that predicts an outage event is the main goal in this scenario. The XGBoost model performs exceptionally well in classification, as seen in Figure. 4.4, with an accuracy rate that approaches 95%. Other tree-based algorithms that retain accuracy levels above 90%, such Random Forest and Decision Tree, come in close second. On the other hand, more computationally sophisticated designs, like as autoencoders and LSTM networks, provide noticeably worse outcomes with significantly lower accuracies.

Research literature supports this observation because blockage-induced traces are easier to analyze regarding oscillatory patterns detection capabilities. Research has shown that threshold-based deterministic approaches [35] offer exceptional accuracy rates of up to 98% through summed periodogram metrics while outperforming sophisticated machine learning (ML) models based on Convolutional Neural Networks (CNNs) and Recurrent Neural Networks (RNNs). [50–52]

4.4 Scenario B: Presence of Micromobility

Furthermore, the dominance of tree-based approaches is highlighted by a thorough analysis of precision and recall metrics, as shown in Figure. 4.1(a) and Figure.

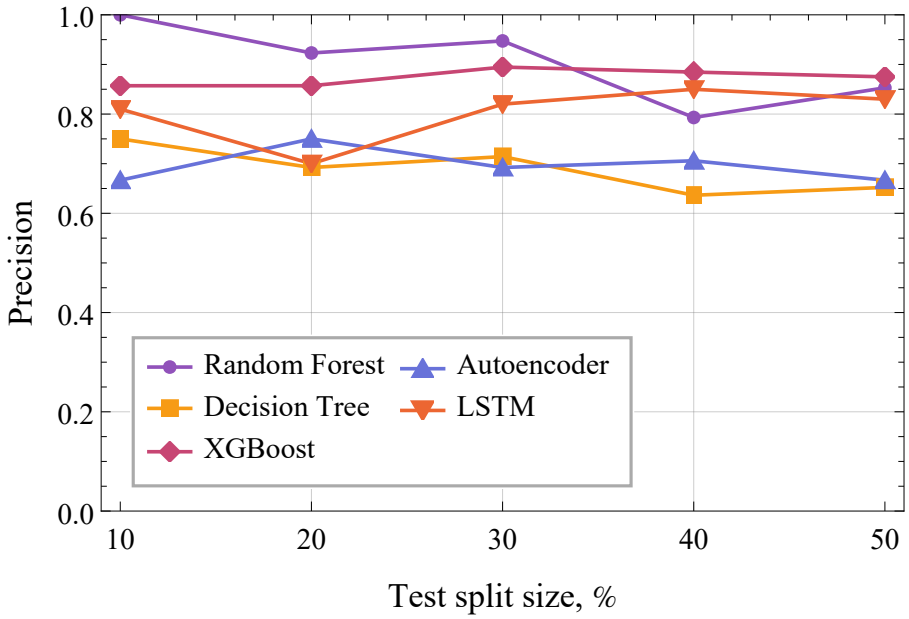

(a) Precision

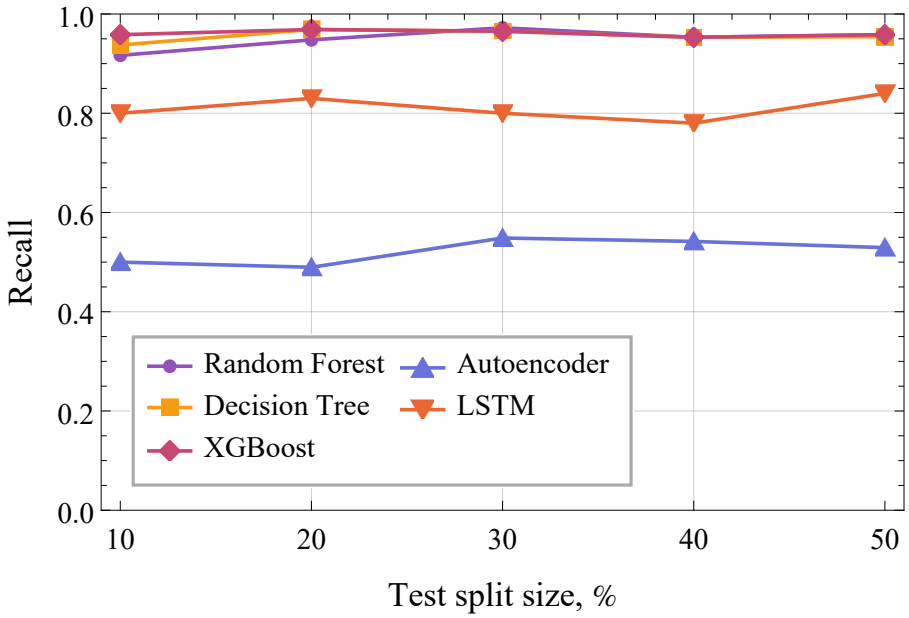

(b) Recall

Figure 4.3 *Precision and recall when detecting blockage with micromobility.*

4.1(b). These algorithms show balanced and resilient precision and recall rates in addition to high accuracy. Crucially, the recall metric continuously outperforms precision by a small margin of about 2–3%. This behavior points to a classifier bias toward minimizing false negatives, which is an important operational characteristic since it avoids needless beam-tracking operations by preventing blockage-induced outages from being mistakenly misclassified as micromobility events. The research results between Figure. 4.1 and Figure. 4.4 demonstrate that the use of advanced

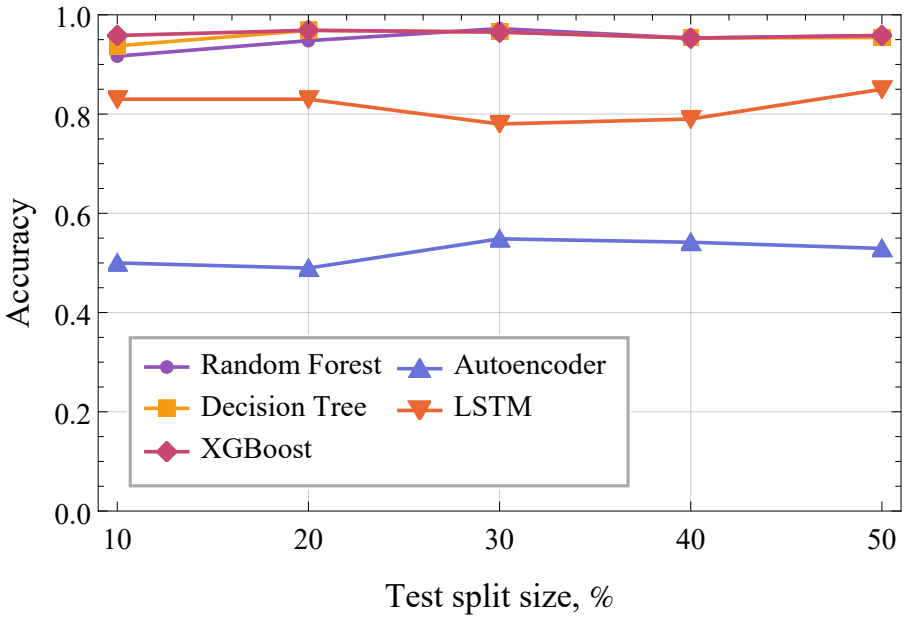

Figure 4.4 *Accuracy when detecting blockage without micromobility.*

neural network structures such as LSTM and Autoencoders does not automatically yield optimal results. Under detailed experimental conditions, these highly complex neural network models both demand substantial computational resources and meticulous parameter adjustment while requiring large training datasets, yet prove less efficient than simpler streamlined approaches.

The analysis examines signal traces that experience both blockage-related and micromobility-induced impairments in their performances Figure. 4.3. Due to micromobility interruptions the detection task becomes more complex because additional interferences emerge.

The data from Figure. 4.2 demonstrates that all algorithms experienced a descent in accuracy levels compared to blockage-only results since micromobility introduced signal fluctuations to the measurements. Random Forest demonstrates superior performance as the top algorithm since it achieves accuracy levels close to 95%, see Figure. 4.2. The accuracy results for XGBoost fall behind random forests because it achieves approximately 90% success. Under mixed impairment conditions LSTM networks demonstrate performance comparable to the other methods by reaching accuracy levels of about 80%. LSTM architecture shows this performance because its ability to model temporal dependencies and handle noisy sequential data.

The analysis of precision and recall shows substantial drops in precision rates , see Figure.4.3(b) while recall values show minimal changes across the algorithms regardless of micromobility presence. The system demonstrates a crucial criterion by showing a preference toward avoiding wrong negative results rather than missing positive results. False negatives represent undetected blockages while false positives

indicate incorrect detection signals. The system introduction of a directional bias serves a strategic purpose by favoring false positives because system safety is more important than false negatives.

All things considered, these experimental results support the more general theory that extremely complicated models do not always produce better results in obstruction and micromobility categorization tasks. Instead, even in difficult and noisy contexts, very straightforward, tree-based ensemble methods like Random Forest—which are distinguished by their inherent robustness, decreased tuning complexity, and computational efficiency frequently produce the best results.

5 Conclusions

In this thesis we addressed two critical issue that causes significant signal loss in high frequency wireless communications as dynamic human body blockage and UE micromobility both of which can lead to outages in mmWave and sub-THz systems. Given that the system response strategies differ based on the type of impairment, accurately differentiating between these causes is essential for robust system design and recovery. To investigate this, we conducted experimental measurements at the 156 GHz sub-THz band and curated a synthetic time-series dataset containing both blockage and micromobility impairments. We proposed a supervised machine learning framework to classify outage events based on the oscillatory behavior of the received signal prior to the outage. Importantly, we applied no transformation to the raw data, allowing models to learn directly from the signal characteristics. Our experimental setup involved real-world measurements at 156 GHz and the generation of synthetic time-series data that captured both blockage and micromobility patterns. Using this dataset, we trained and evaluated a range of machine learning models to classify the impairments based on signal oscillation patterns just before an outage occurs. Our results show that machine learning models can indeed differentiate between outages caused by blockage and micromobility. Among the various techniques explored, tree-based ensemble models, particularly Random Forest, achieved the best performance. This model reached up to 95% classification accuracy, with high recall values indicating minimal false negatives for blockage detection even when micromobility impairments were present. This high recall is crucial as it minimizes the risk of misinterpreting a blockage-induced outage as micromobility. To explore this issue, we posed the following research questions:

1. Can a machine learning based model help differentiate between dynamic human body blockage and UE micromobility in high frequency wireless systems like mmWave and sub-THz?

2. If so, what kind of performance such as accuracy and false detection rates can be expected from different machine learning algorithms?

In response to the first research question, our findings confirm that machine learning models can successfully differentiate between blockage-induced and micromobility induced outages. The models could identify subtle variations in the signal's temporal behavior that correspond to each impairment, even when both occur simultaneously. Regarding the second research question, we observed that tree-based ensemble models, particularly Random Forest, offered the best trade-off between accuracy and computational efficiency. The Random Forest classifier achieved up to 95% accuracy, along with high recall values, indicating its robustness in detecting

blockage events without misclassifying micromobility-related outages. Interestingly, more complex neural network models did not outperform simpler models and required longer training times and fine-tuning, suggesting they may be unnecessary for this task.

In summary, this thesis presents an effective and lightweight ML-based solution for impairment classification in sub-THz systems, which can support the development of more intelligent and responsive communication networks in future 6G deployments.

Bibliography

[1] A. Shurakov, D. Moltchanov, A. Prikhodko, A. Khakimov, E. Mokrov, V. Begishev, I. Belikov, Y. Koucheryavy, and G. Gol'tsman, "Empirical blockage characterization and detection in indoor sub-thz communications," *Computer Communications*, vol. 201, pp. 48–58, 2023.

[2] K. Kumaravel, "Comparative study of 3G and 4G in mobile technology," *International Journal of Computer Science Issues (IJCSI)*, vol. 8, no. 5, p. 256, 2011.

[3] S. Borkar and H. Pande, "Application of 5G next generation network to internet of things," in *2016 International Conference on Internet of Things and Applications (IoTA)*, pp. 443–447, IEEE, 2016.

[4] P. Shah, "The future of iot and 5G: Unlocking new possibilities in connectivity," *Advances in Computer Sciences*, vol. 6, no. 1, 2023.

[5] Ericsson, "5G wireless access: An overview," 2021. Accessed: 2021-11-01.

[6] M. Polese, M. Giordani, and M. Zorzi, "3GPP nr: The standard for 5G cellular networks," in *5G Italy White eBook: From Research to Market*, Rome, Italy: 5G Italy, 2018.

[7] Ericsson, "Ericsson report. 5G evolution: 3GPP releases 16 and 17 overview," 2021. Accessed: 2021-11-01.

[8] IEEE International Symposium on Personal, Indoor and Mobile Radio Communications, "Panel 5: Evolution of 5G mmwave," 2021. Accessed: 2021-11-01.

[9] 3GPP, "NR; Physical Channels and Modulation (Release 15)," 3GPP Technical Report TR 38.211, 3GPP, Sophia Antipolis, France, Dec. 2017.

[10] 3GPP, "3GPP: Advanced plans for 5G," 2021. Accessed: 2021-11-01.

[11] V. Petrov, D. Solomitckii, A. Samuylov, M. A. Lema, M. Gapeyenko, D. Moltchanov, S. Andreev, V. Naumov, K. Samouylov, M. Dohler, *et al.*, "Dynamic multi-connectivity performance in ultra-dense urban mmwave deployments," *IEEE Journal on Selected Areas in Communications*, vol. 35, no. 9, pp. 2038–2055, 2017.

[12] J. G. Andrews, S. Buzzi, W. Choi, S. V. Hanly, A. Lozano, A. C. K. Soong, and J. C. Zhang, "What will 5G be?," *IEEE Journal on Selected Areas in Communications*, vol. 32, no. 6, pp. 1065–1082, 2014.

[13] D. Moltchanov, E. Sopin, V. Begishev, A. Samuylov, Y. Koucheryavy, and K. Samouylov, "A tutorial on mathematical modeling of 5G/6G millimeter wave and terahertz cellular systems," *IEEE Communications Surveys Tutorials*, vol. 24, no. 2, pp. 1072–1116, 2022.

[14] K. Yang, Z. Zhao, J. Liu, and Q. Huo Liu, "Robust adaptive beamforming using an iterative fft algorithm," *Signal Processing*, vol. 96, pp. 253–260, 2014.

[15] X. Gao, L. Dai, S. Han, C.-L. I, and R. W. Heath, "Energy-efficient hybrid analog and digital precoding for mmwave mimo systems with large antenna arrays," *IEEE Journal on Selected Areas in Communications*, vol. 34, pp. 998–1009, Apr. 2016.

[16] 3GPP, "Channel model for frequency spectrum above 6 ghz," 3GPP Technical Report TR 38.900, 3rd Generation Partnership Project (3GPP), 2016. Release 14.

[17] C.-X. Wang, J. Wang, S. Hu, Z. H. Jiang, J. Tao, and F. Yan, "Key technologies in 6G terahertz wireless communication systems: A survey," *IEEE Vehicular Technology Magazine*, vol. 16, pp. 27–37, Dec. 2021.

[18] Y. Niu, Y. Li, D. Jin, L. Su, and A. V. Vasilakos, "A survey of millimeter wave communications (mmwave) for 5G: opportunities and challenges," *Wireless networks*, vol. 21, pp. 2657–2676, 2015.

[19] T. S. Rappaport, J. N. Murdock, and F. Gutierrez, "State of the art in 60-ghz integrated circuits and systems for wireless communications," *Proceedings of the IEEE*, vol. 99, no. 8, pp. 1390–1436, 2011.

[20] E. Golos, A. Daraseliya, E. Sopin, V. Begishev, and Y. Gaidamaka, "Optimizing service areas in 6g mmwave/thz systems with dual blockage and micromobility," *Mathematics*, vol. 11, no. 4, p. 870, 2023.

[21] M. Giordani, M. Polese, M. Mezzavilla, S. Rangan, and M. Zorzi, "Toward 6G networks: Use cases and technologies," *IEEE communications magazine*, vol. 58, no. 3, pp. 55–61, 2020.

[22] N. Rajatheva, I. Atzeni, E. Björnson, A. Bourdoux, S. Buzzi, J.-B. Dore, S. Erkucuk, M. Fuentes, K. Guan, Y. Hu, X. Huang, J. Hulkkonen, J. Jornet, M. Katz, R. Nilsson, E. Panayirci, K. Rabie, N. Rajapaksha, M. Salehi, and W. Xu, "White paper on broadband connectivity in 6G," 04 2020.

[23] D. Moltchanov, A. Samuylov, V. Petrov, M. Gapeyenko, N. Himayat, S. Andreev, and Y. Koucheryavy, "Improving session continuity with bandwidth

reservation in mmwave communications," *IEEE Wireless Communications Letters*, vol. 8, no. 1, pp. 105–108, 2019.

[24] S. Jun, Y.-s. Choi, and H. Chung, "Considerations on multi-radio multi-connectivity in 6G system," in *2022 13th International Conference on Information and Communication Technology Convergence (ICTC)*, pp. 2041–2043, 2022.

[25] A. E. Kalor, G. Durisi, S. Coleri, S. Parkvall, W. Yu, A. Mueller, and P. Popovski, "Wireless 6G connectivity for massive number of devices and critical services," *Proceedings of the IEEE*, pp. 1–23, 2024.

[26] N. Stepanov, A. Turlikov, V. Begishev, Y. Koucheryavy, and D. Moltchanov, "Accuracy assessment of user micromobility models for thz cellular systems," 2021.

[27] V. Begishev, E. Sopin, D. Moltchanov, R. Kovalchukov, A. Samuylov, S. Andreev, Y. Koucheryavy, and K. Samouylov, "Joint use of guard capacity and multiconnectivity for improved session continuity in millimeter-wave 5G nr systems," *IEEE Transactions on Vehicular Technology*, vol. 70, no. 3, pp. 2657–2672, 2021.

[28] V. Begishev, D. Moltchanov, E. Sopin, A. Samuylov, S. Andreev, Y. Koucheryavy, and K. Samouylov, "Quantifying the impact of guard capacity on session continuity in 3GPP new radio systems," *IEEE Transactions on Vehicular Technology*, vol. 68, no. 12, pp. 12345–12359, 2019.

[29] M. S. Alamgir and B. Kelley, "6G vision-intelligent millimeter-wave systems on high-altitude platform stations," in *2024 IEEE 15th Annual Ubiquitous Computing, Electronics Mobile Communication Conference (UEMCON)*, pp. 539–547, 2024.

[30] J. E. Galeote-Cazorla, A. Ramírez-Arroyo, J. Molina-García-Pardo, M. Martínez-Inglés, and J. F. Valenzuela-Valdés, "Experimental assessment of human blockage at sub-thz and mmwave frequency bands," *arXiv preprint arXiv:2411.13191*, 2024.

[31] M. Gapeyenko, A. Samuylov, M. Gerasimenko, D. Moltchanov, S. Singh, E. Aryafar, S.-p. Yeh, N. Himayat, S. Andreev, and Y. Koucheryavy, "Analysis of human-body blockage in urban millimeter-wave cellular communications," in *2016 IEEE International Conference on Communications (ICC)*, pp. 1–7, 2016.

[32] D. Solomitckii, Q. C. Li, T. Balercia, C. R. C. M. da Silva, S. Talwar, S. Andreev, and Y. Koucheryavy, "Characterizing the impact of diffuse scattering in urban millimeter-wave deployments," *IEEE Wireless Communications Letters*, vol. 5, no. 4, pp. 432–435, 2016.

[33] A. Alyosef, S. Rizou, Z. D. Zaharis, P. I. Lazaridis, A. M. Nor, O. Fratu, S. Halunga, T. V. Yioultsis, and N. V. Kantartzis, "A survey on the effects of human blockage on the performance of mm wave communication systems," *2022 IEEE International Black Sea Conference on Communications and Networking (BlackSeaCom)*, pp. 249–253, 2022.

[34] E. Golos, A. Daraseliya, E. Sopin, V. Begishev, and Y. Gaidamaka, "Optimizing service areas in 6G mmwave/thz systems with dual blockage and micromobility," *Mathematics*, vol. 11, no. 4, 2023.

[35] F. Zhinuk, A. Gaydamaka, D. Moltchanov, and Y. Koucheryavy, "Spectral-based proactive blockage detection for sub-thz communications," *IEEE Communications Letters*, 2024.

[36] N. Stepanov, D. Moltchanov, V. Begishev, A. Turlikov, and Y. Koucheryavy, "Statistical analysis and modeling of user micromobility for thz cellular communications," *IEEE Transactions on Vehicular Technology*, vol. 71, no. 1, pp. 725–738, 2021.

[37] V. Petrov, D. Moltchanov, Y. Koucheryavy, and J. M. Jornet, "Capacity and outage of terahertz communications with user micro-mobility and beam misalignment," *IEEE Transactions on Vehicular Technology*, vol. 69, no. 6, pp. 6822–6827, 2020.

[38] M. Gapeyenko, A. Samuylov, M. Gerasimenko, D. Moltchanov, S. Singh, M. R. Akdeniz, E. Aryafar, N. Himayat, S. Andreev, and Y. Koucheryavy, "On the temporal effects of mobile blockers in urban millimeter-wave cellular scenarios," *IEEE Transactions on Vehicular Technology*, vol. 66, no. 11, pp. 10124–10138, 2017.

[39] M. Gapeyenko, V. Petrov, D. Moltchanov, S. Andreev, N. Himayat, and Y. Koucheryavy, "Flexible and reliable UAV-assisted backhaul operation in 5G mmWave cellular networks," *IEEE Journal on Selected Areas in Communications*, vol. 36, no. 11, pp. 2486–2496, 2018.

[40] L. Breiman, "Random forests," *Machine learning*, vol. 45, pp. 5–32, 2001.

[41] "Classification based on decision tree algorithm for machine learning," *Journal of Applied Science and Technology Trends*, vol. 2, pp. 20–28, Mar. 2021.

[42] Y. Lu, T. Ye, and J. Zheng, "Decision tree algorithm in machine learning," in *2022 IEEE International Conference on Advances in Electrical Engineering and Computer Applications (AEECA)*, pp. 1014–1017, 2022.

[43] P. Carmona, A. Dwekat, and Z. Mardawi, "No more black boxes! explaining the predictions of a machine learning xgboost classifier algorithm in business failure," *Research in International Business and Finance*, vol. 61, p. 101649, 2022.

[44] H. Torabi, S. L. Mirtaheri, and S. Greco, "Practical autoencoder based anomaly detection by using vector reconstruction error," *Cybersecurity*, vol. 6, Jan 2023.

[45] M. A. Kramer, "Nonlinear principal component analysis using autoassociative neural networks," *AIChE Journal*, vol. 37, no. 2, pp. 233–243, 1991.

[46] P. Vincent, H. Larochelle, Y. Bengio, and P.-A. Manzagol, "Stacked denoising autoencoders: Learning useful representations in a deep network with a local denoising criterion," *Journal of Machine Learning Research*, vol. 11, no. 12, pp. 3371–3408, 2010.

[47] P. Malhotra, L. Vig, G. Shroff, P. Agarwal, *et al.*, "Long short term memory networks for anomaly detection in time series," in *Proceedings*, vol. 89, p. 94, 2015.

[48] B. Juba and H. S. Le, "Precision-recall versus accuracy and the role of large data sets," in *Proceedings of the AAAI Conference on Artificial Intelligence*, vol. 33, pp. 4039–4048, July 2019.

[49] 3GPP, "NR; Physical layer; General description (release 18)," 3GPP technical report 38.201, 3rd Generation Partnership Project (3GPP), Dec. 2023.

[50] S. Moon, H. Kim, Y.-H. You, C. H. Kim, and I. Hwang, "Deep neural network for beam and blockage prediction in 3GPP-based indoor hotspot environments," *Wireless Personal Communications*, pp. 1–20, 2022.

[51] S. Wu, M. Alrabeiah, C. Chakrabarti, and A. Alkhateeb, "Blockage prediction using wireless signatures: Deep learning enables real-world demonstration," *IEEE Open Journal of the Comm. Soc*, vol. 3, pp. 776–796, 2022.

[52] S. Wu, M. Alrabeiah, A. Hredzak, C. Chakrabarti, and A. Alkhateeb, "Deep learning for moving blockage prediction using real mmWave measurements," in *IEEE ICC 2022*, pp. 3753–3758, IEEE, 2022.